Catalysis Science & Technology

Accepted Manuscript

This is an *Accepted Manuscript*, which has been through the Royal Society of Chemistry peer review process and has been accepted for publication.

Accepted Manuscripts are published online shortly after acceptance, before technical editing, formatting and proof reading. Using this free service, authors can make their results available to the community, in citable form, before we publish the edited article. We will replace this *Accepted Manuscript* with the edited and formatted *Advance Article* as soon as it is available.

You can find more information about *Accepted Manuscripts* in the Information for Authors.

Please note that technical editing may introduce minor changes to the text and/or graphics, which may alter content. The journal's standard Terms & Conditions and the Ethical guidelines still apply. In no event shall the Royal Society of Chemistry be held responsible for any errors or omissions in this *Accepted Manuscript* or any consequences arising from the use of any information it contains.

ROYAL SOCIETY OF CHEMISTRY

www.rsc.org/catalysis

CREATED USING THE RSC LaTeX PCCP ARTICLE TEMPLATE – SEE www.rsc.org/electronicfiles FOR DETAILS
ARTICLE TYPE www. rsc.org/xxxxxx | XXXXXXXX

Review: Monoclinic zirconia, its surface sites and their interaction with carbon monoxide

Sonja Kouva,[*,a] **Karoliina Honkala,** [b] **Leon Lefferts,**[a,c] **and Jaana Kanervo**[a]

Received Xth XXXXXXXXXX 2015, Accepted Xth XXXXXXXXX 201X
First published on the web Xth XXXXXXXXXX 201X
DOI: 10.1039/b000000x

This review concerns monoclinic zirconia, its surface sites and their probing with carbon monoxide. The surface sites and their modifications using thermal treatments with vacuum or reactive gases are also included. In this work, we present information on the nature and manipulation of hydroxyl species and their quantities on the surface, the different types of cationic sites where CO is adsorbed linearly and their energetics, as well as the surface sites and dynamics of formate formation. We also compare the surface concentrations of the different surface species to better understand the extent and nature of the interactions. Finally, we discuss some of the remaining open questions and how to approach them.

1 Introduction

Zirconium oxide has gained interest both as a catalyst support and a catalyst on its own, mostly due to its weak acid and basic sites[1] and stability under oxidizing and reducing atmospheres[2]. It has been an interesting catalyst material especially for biomass-related reactions that are actively investigated, as the future is bright for non-fossil fuels and chemicals. Biomass-related reaction networks usually include carbon oxides, as both carbon and oxygen are largely abundant in the starting material.

Monoclinic zirconia (also known as baddeleyite) is an oxide typically covered with hydroxyl species, similar to many metal oxides[3] used as catalysts and catalyst support materials. The structure of monoclinic zirconia provides a more versatile surface than the other polymorphs (cubic, tetragonal) due to a less symmetrical lattice[4]. The surface sites on monoclinic zirconia include hydroxyls[5], oxygen vacancies[6], coordinatively unsaturated (c.u.s.) Zr–O pairs[7], and Lewis acid sites (Zr^{3+}, Zr^{4+})[8]. The hydroxyl groups on the surface can be manipulated by thermal treatment in vacuum or in different atmospheres[9], which are often necessary for catalytic applications, *e.g.*, in methanol synthesis[10]. Additionally, monoclinic zirconia has been suggested as a support for water-gas shift reaction catalysts with gold, platinum and copper[11–13], and for reforming with platinum, nickel, cobalt and copper[14,15].

Since 2006, monoclinic zirconia has been prepared also in nanoshapes, including nanorods[16,17] and nanosheets[16]. Using the nanoshapes in catalysis might be beneficial due to their well-defined surface sites; thus their selectivity might be more easily linked to the exposed surfaces than those of traditional catalysts in polycrystalline form.

Carbon monoxide interacts with monoclinic zirconia both on the clean surface with few or no hydroxyls[18], as well as on the hydroxylated surface[19,20]. The surface hydroxyl groups seem to play an important role in the interaction of CO with zirconia: as a site for forming formates[5,7,20–23] and bicarbonates[22,24–26] but also inhibiting the formation of adsorbed linear CO species[27]. The main adsorbed CO species are linearly adsorbed CO at room temperature and below and formate species above 100 °C, the first one desorbing reversibly[27] and the second one decomposing both reversibly back to gas-phase CO and irreversibly to CO_2 and H_2[20,21,28].

The interaction of carbon monoxide with zirconium oxide has been studied actively since the 1970s[5,18,21,23,29,30]. Due to differences in zirconia materials and their pretreatments, experimental setups and conditions, interpreting and comparing the obtained results is not straightforward. Most of the studies on the interaction with CO have been carried out using infrared spectroscopy[5,18,19,22–24]. However, studies using other techniques, such as temperature-programmed methods[20,21,28,30], calorimetry[27,31,32], and gravimetry[33,34], as well as theoretical studies[22,28] have been published.

The focus of this work is in the monoclinic polymorph of zirconia instead of the whole spectrum of zirconia materials: doped (including sulphated), tetragonal and cubic zirconia, to name the most significant zirconias excluded from this review. This choice is made for simplicity and clarity, as monoclinic and tetragonal zirconias differ in, *e.g.*, surface hydroxyl species[7,25] and acidity/basicity[7,24,30], further demonstrated in their interactions with CO[7,25,30] and in their catalytic activity, *e.g.*, in water-gas shift[11,12]. More information can also be found in the reviews by Dyrek *et al.*[35] and Hadjiivanov[36].Most of the pre-1993 works included in this paper were reviewed 20 years ago by Nawrocki *et al.*[37] in the context of chromatography; this review is providing an update

Catalysis Science & Technology Accepted Manuscript

with work reported since 1993, from the perspective of catalysis.

2 Preparation, structure, and surfaces

2.1 Preparation

Zirconium oxide can be prepared, *e.g.*, *via* hydrolysis from zirconium isopropylate ($Zr(OCH(CH_3)_2)_4$)[8,18,27,38–40] or zirconium oxychloride ($ZrOCl_2$)[25,30,41–43], and also from zirconium oxynitrate ($ZrO(NO_3)_2$)[42–44] and zirconium tetrachloride ($ZrCl_4$)[10,45]. Yamaguchi introduces the processes starting from natural ores (zircon ($ZrSiO_4$), baddeleyite) to zirconium oxide preparation[2]. Origin of the zirconia samples referred to in this review, with their preparation conditions and surface areas are presented in Table 1 to aid the reader by presenting the key properties of the materials used. Note that the applied pretreatment conditions might differ from the preparation conditions.

2.2 Crystal structure and surfaces

The unit cell of monoclinic zirconia is face-centered (space-group C^5_{2h}), consisting of 4 Zr atoms and 8 O atoms[72]. In the bulk all Zr atoms are seven-fold coordinated to three three-fold coordinated oxygen atoms and four four-fold coordinated oxygen atoms[73]. Based on theory, the coordination numbers on the surface differ, *e.g.*, on the $(\bar{1}11)$ surface some of the zirconium atoms are only six-fold coordinated and some of the oxygen atoms are three- or two-fold coordinated instead of four- or three-fold coordination[74]. On the $(\bar{1}11)$ surface, some zirconium atoms can be even five-fold coordinated[74]. The experimentally determined lattice parameters are $a = 5.17$Å, $b = 5.23$Å, and $c = 5.34$Å, and the angle $\gamma = 99.3°$[75].

Monoclinic zirconia has altogether nine inequivalent crystalline directions: [001], [010], [100], [110], [101], [011], $[\bar{1}01]$, [111] and $[\bar{1}11]$[4]. Warble reported (110), (100) and (111) surfaces to be exhibited in transmission electron microscopy (TEM)[76]. The (111)[39,40], (001)[39,40] and (011)[40] planes have been reported based on high-resolution TEM (HRTEM) images. Theoretically, the most stable surface for monoclinic zirconia is the $(\bar{1}11)$ surface[4]. The difference between the theoretically most stable surfaces and the experimentally observed surfaces might be due to inaccuracy in either method, and it is not clear whether the particle size or, *e.g.*, the degree of surface hydration play a role. In nanocrystals, the (011) surface seems most abundant in TEM, while also $(\bar{1}11)$, (111) and (001) surfaces have been observed[77]. The ideal (111), $(\bar{1}11)$, (001) and (011) surfaces are shown in Figure 1. The atom positions are those of the bulk structure assuming no reconstruction takes place.

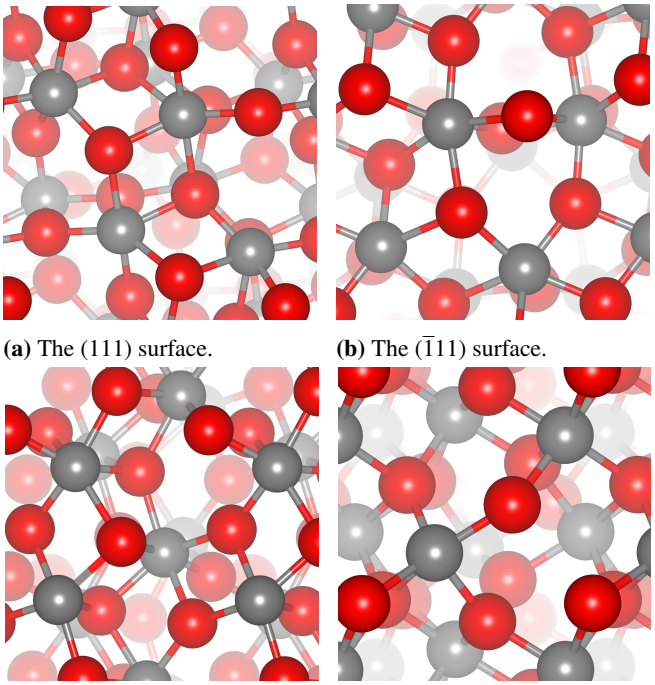

(a) The (111) surface. **(b)** The $(\bar{1}11)$ surface. **(c)** The (011) surface. **(d)** The (001) surface.

Fig. 1 Ideal surfaces of monoclinic ZrO_2, top view, Zr atoms are grey and O atoms red. The atoms further in the lattice are shaded lighter than those on the surface. The surfaces were visualized using VESTA software[78].

Jung *et al.* report that the crystallographic structure of zirconia, instead of crystallite size or calcination temperature, is the most significant factor for determining the nature and density of the surface sites suitable for CO_2 and NH_3 adsorption, *i.e.*, the basic and acidic surface sites[41]. Monoclinic zirconia has a higher CO adsorption capacity than tetragonal ZrO_2, which is attributed to its higher Lewis acidity and basicity[30]. The tetragonal structure is more symmetrical than the monoclinic one[4], leading to a smaller number of different surfaces and thus possibly also to less versatile surface site types.

Thermal treatment tends to increase the crystal size of monoclinic zirconia. Increasing the calcination temperature by $300-500\,°C$ can lead to a particle size of three or even four times the original[40,64]. Auger electron spectroscopy (AES)[79] shows that the surface O/Zr ratio decreases from the stoichiometric 2 down to 1.1 with evacuation at 427 °C and 727 °C, respectively. The surface reduction is very fast, and extending the time to one hour in ultra-high vacuum (UHV) does not affect the surface[79]. With H_2 the surface seems unreducible even at 900 Torr and 900 °C while atomic hydrogen reduces the surface already at 750 °C and H_2 pressure of 5 μTorr prior to atomization[80]. The ineffectiveness of H_2 compared to UHV in surface reduction is rather unexpected, yet atomic hydrogen

Catalysis Science & Technology Accepted Manuscript

This journal is © The Royal Society of Chemistry [year]

Table 1 Origin, preparation conditions and surface area of the zirconia samples [a]

Material	T_{calc} (°C)	Atmosphere	A_s (m^2/g)	Ref.
Decomposition of $ZrO(NO_3)_2 \cdot xH_2O$	300 & 300	air & 10% H_2	20	42,43
Hydrolysis of $ZrOCl_2$	600	air, 4h	-	9
Hydrolysis of $ZrOCl_2$	300 & 700	O_2, 5h	110 & 19	25,30
Hydrolysis of $ZrOCl_2$	700 & 300 – 550	calc. & vacuum, air (1h), H_2, vacuum	44	29
Hydrolysis of $ZrOCl_2$	800 & 1000	vacuum, 10 min & air, 6h	-	46
Hydrolysis of $ZrO(NO_3)_2$	500 & 800	air, 5h & vacuum, 5h	-	47
Hydrolysis of $ZrO(NO_3)_2$	700 & 500 & 700	calc., 3h & O_2, 10h & vac., 20 min	58 [c]	48
Hydrolysis of $ZrO(NO_3)_2$	500 & 500 & 730	calc., 3h & O_2, overnight & vac., 20 min	-	49
Hydrolysis of $ZrO(NO_3)_2$	530 / 710	air, 3h	70 / 58	26
Hydrolysis of Zr isopropylate	447	calcination	81[c]	50
Hydrolysis of Zr isopropylate	447 & 597	calcination & vacuum, 2h	82	18
	447 & 27 – 397	calcination & vacuum, 2h	92 (397 °C)	18
Hydrolysis of Zr isopropylate	447 & 797	calc. & vac., 2h + 50 torr O_2, 30 min	36	27
	447 & 397 – 597	calc. & vac., 2h + 50 torr O_2, 30 min	80–90	27
Hydrolysis of Zr isopropylate	447 & 400 & RT & 250 – 600	calc. & vac. + O_2 & H_2O vapor & vac., 2h	-	38
Hydrolysis of Zr isopropylate	397 & 100 – 600	air & vacuum, 2h + O_2	-	8
Hydrolysis of Zr isopropylate	397 & *e.g.* 597 & *e.g.* 597	calc. & vacuum, 2h & O_2, 30 min	-	51
Hydrolysis of Zr isopropylate	597 & 197 – 597	calc. & vacuum	78	39
	997 & 197 – 597	calc. & vacuum	10	39
Hydrolysis of Zr isopropylate	600 / 800 / 900 & 27 – 800	air, 3h & vacuum	55 / 35 / 20 [c]	40
Hydrolysis of Zr isopropylate	400 & 400	calcination & vacuum	84	52
Hydrolysis of Zr propylate	400	O_2 & vacuum	200 – 220	53
Hydrolysis of Zr propylate	400	O_2, 1h & He 30 min	200	20
Hydrolysis of Zr propylate	440	O_2, 2h	200 – 220	54
Hydrolysis of Zr propylate	440	air, 12h	120	55
Microemulsion from $ZrOCl_2$	500 – 1200	annealing	1.6 – 44.9	31
NH_3 hydrolysis of $ZrOCl_2$	120 & 400	drying & preheating	-	56
NH_3 hydrolysis of $ZrOCl_2$	550 & 550	air, 2h & N_2, 7h	70	57
NH_3 hydrolysis of $ZrOCl_2$	550	air, 1h	56	58
NH_3 hydrolysis of $ZrOCl_2$	500	air, 6h	57	59,60
NH_3 hydrolysis of $ZrOCl_2$	600	vacuum	41	7
NH_3 hydrolysis of $ZrOCl_2$	100 & 700	O_2, 5h	19	41
NH_3 hydrolysis of dissolved $ZrCl_4$	600 – 900	air, 2 – 6h	8.2 – 30	45
NH_3 hydrolysis of dissolved $ZrCl_4$	600	O_2	30 – 36	10
NH_3 hydrolysis of $Zr(NO_3)_4$	500	air, 2 – 3h	80 [b]	44
PICA process	700	air, 2h	33	34
$ZrO(NO_3)_2$ precipitation with hydrazine	1450 & 800	air & vacuum	1.0	32
A.D Mackay / nuclear grade	500	vacuum	23.7	33,61
Alfa Aesar	> 1200 & 800	air & vacuum	1.6	32
Alfa Aesar	900	air	10.4	62
Alfa-Ventron	620	O_2, 0.5 h & He, 0.25 h & H_2, 0.5 h	5.8[c]	21
Alfa-Ventron	500	O_2, overnight	5.8 [d]	19
Criceram / $ZrCl_4$ + H_2O vapor	877/903	air, 24h / 30% O_2 + 70% H_2O, 24h	6 / 4.2	63
Daiichi Kigenso Kagaku Kogyo (RC100)	400	air, 15h	71	64
Degussa / flame hydrolysis	600 – 800	air or vacuum	37 ± 1 [c]	65
Degussa	450	air, 4h	40	66
Gimex Technical Ceramics (RC-100)	600 & 400	He, 24h & H_2, 30 min	-	23
Magnesium Elektron (E-10 powder)	-	vacuum	14	24
MEL EC0100	580	O_2, 2h	47	22,67
MEL $Zr(OH)_4$	RT/150/300/500	vacuum	66.6 – 537	68
MEL $Zr(OH)_4$	450 & 600	air, 16h & O_2/inert, 2h	90	28
Nanotek	-	-	78	6
Saint-Gobain NorPro	-	-	52	69
Commercial $Zr(OH)_4$	700	calcination, 6h	12	70

details about their zirconium oxide material.

[b] Surface area value reported prior to calcination.

[c] Surface area value reported prior to wafer pressing.

This journal is © The Royal Society of Chemistry [year]

Catalysis Science & Technology Accepted Manuscript

seems to be a better reductant than molecular hydrogen. Based on the literature, the mechanism for oxygen removal remains unclear; is it removed as O_2 or perhaps through dehydroxylation *via* multicoordinated OH groups, as shown in Eq. 1:

$$\text{multi-OH} + \text{multi-OH} \leftrightarrow O_{lattice} + \text{vacancy} + H_2O. \quad (1)$$

The presence of Zr^{3+} sites has been proposed based on electron paramagnetic resonance (EPR)[8,46,51,57]. The Zr surface cations have been probed with N_2O, it decomposes on Zr^{3+} already at room temperature but also at higher temperatures, and reversibly adsorbs on Zr^{4+} sites[6]. Vacuum treatment at above 600 °C is sufficient to initiate formation of oxygen vacancies[81] and reduction of cations from Zr^{4+} to Zr^{3+} [6,81]. Hydrogen treatment at 700 °C also transforms some of the Zr^{4+} sites to Zr^{3+} sites[81], but with hydrogen treatment at 600 °C, the amount of Zr^{3+} sites does not increase[9] in agreement with the low reducibility with H_2 mentioned previously. If the sample has been vacuum-activated at 400 °C, hydration quenches the defect centers (Zr^{3+}) and the defects have to be re-created with evacuation[8]. If the sample has been vacuum-activated at 800 °C, there are two options: (1) the defect centers are quenched but they are easier to re-create on a sintered surface, or (2) the defect centers are not quenched, rather coordinatively saturated with water and dehydration restores their coordinatively unsaturated state[8]. Based on EPR, the most exposed Zr^{3+} are transformed to Zr^{4+} when in contact with water (200 °C, 18 torr H_2O) but the others are coordinatively saturated with water and remaining Zr^{3+} [8] .

Syzgantseva *et al.* have calculated the formation energies for oxygen vacancies, and based on those the zirconia $(\bar{1}11)$ surface is less reducible than the $(\bar{1}01)$ surface[82], in line with the stability observation by Christensen and Carter[4]. When comparing to other oxides, the oxygen vacancy formation energy on the zirconia surface is $820-880$ kJ/mol and in the bulk *ca.* 860 kJ/mol, whereas those for titania, which is considered a reducible oxide, are $530-580$ kJ/mol on the surface and 670 kJ/mol in the bulk[82]. Syzgantseva *et al.* have also predicted the conditions necessary to create oxygen vacancies with surface hydrogenation followed by desorption of water (temperature above 927 °C and H_2O/H_2 pressure ratio below 10^{-5})[82]. They conclude that water desorption takes place already at milder conditions, thus the simplifications in their computations required for, *e.g.*, surface models might cause the discrepancy between theory and experiments[82].

The oxygen mobility, dissociation and recombination on zirconia among other oxide materials were probed by Martin and Duprez[66]. Isotopic oxygen exchange experiments between $^{16}O_2$ and $^{18}O_2$ showed surface oxygen exchange at $380-780$ °C[66]. The maximum O-exchange rate was at 530 °C and the exchange rate was further expedited in the presence of Rh or Pt on the surface[66]. The exchange is attributed to c.u.s. Zr^{3+} centers created by vacuum thermal treatment and their ability to dissociate molecular oxygen[66]. The number of exchanged oxygens on ZrO_2 was found to be greater than the theoretical number of surface oxygen species implying that bulk oxygen atoms participated in the exchange[66].

3 Hydroxyl species and the interaction of water and hydrogen on monoclinic zirconia

Dissociative adsorption of water on monoclinic zirconia is exothermic, occurring already at room temperature[31,69]. Therefore the surfaces of zirconia are hydroxylated under ambient and in most reactive atmospheres. In this section, different types of OH groups are discussed, followed by methods of manipulating the hydroxyl species on the surface of zirconia.

3.1 Nature, density and probing of hydroxyl species

Typical hydroxyl sites reported on monoclinic zirconia include terminal OH groups (also known as monocoordinated OH) and tribridged OH groups, first assigned by Tsyganenko and Filimonov as a part of a wider study on different oxides including cerium, hafnium, magnesium, nickel, cobalt and several other oxides[3,71]. Schematic drawings of the hydroxyl groups are presented in Fig. 2. The latter species has been assigned either tribridged[7,25,70,71], bibridged[29,53,61,63] or simply presumed as multicoordinated OH groups[18,19,23,59]. In this work, the term multicoordinated is generally used to refer to this species.

Fig. 2 Terminal and tribridged hydroxyl species.

The terminal and multicoordinated hydroxyl species are usually observed in IR spectroscopy at $3780-3760$ cm^{-1} and $3690-3650$ cm^{-1}, respectively[7,19,50,61,71], as shown in Table 2 and Figure 3. Jacob *et al.* assign the bands to OH groups related to trigonally coordinated O^{2-} anions (*ca.* 3774 cm^{-1}) and to tetrahedrally coordinated O^{2-} anions (*ca.* 3668 cm^{-1})[65], however, without further evidence. Yamaguchi *et al.* suggested that the bands at 3780 cm^{-1} and 3680 cm^{-1} would be isolated hydroxyls (as opposed to hydrogen-bonded ones) of bridged and terminal type adapting the interpretation for rutile, a type of TiO_2[59]. The occurrence of a band at $3740-3720$ cm^{-1} is typically interpreted as **a** sign of tetragonal phase and its bibridged hydroxyl. Yet the band of terminal OH (typically at $3780-3760$ cm^{-1}) shifts towards lower

Catalysis Science & Technology Accepted Manuscript

This journal is © The Royal Society of Chemistry [year]

wavenumbers (even down to 3680 cm^{-1}) with increasing degree of hydration due to hydrogen bonding [18] and at that point the multicoordinated OH band is even below 3600 cm^{-1} [40], as suggested already by Tret'yakov *et al.* [44]. Thus interpreting the hydroxyl band position must be done carefully, considering the possibility of hydrogen bonding at higher degrees of hydration. Tsyganenko and Filimonov also report an IR band at 3380 cm^{-1}, assigned to hydrogen-bonded hydroxyl groups [3,71]. Unresolved broad bands at $3600-2800$ cm^{-1} are assigned to hydrogen-bonded polynuclear water species [61] based on the IR spectra of hydrogen bonding of water [83]. The hydrogen bonding is suggested to occur between molecularly adsorbed water and the hydroxyl groups [18,33,42,53].The OH wavenumber and thermal stability depend on the crystalline phase of zirconia [9]; thus impurities in the crystalline phase can lead to misinterpretations.

Table 2 Experimentally and theoretically determined ν(OH) wavenumbers

Terminal cm^{-1}	Bibridged cm^{-1}	Tribridged cm^{-1}	H-bonded cm^{-1}	Ref.
		Experimental		
3770		3670	3380	3,71
3776		3667		50
3772		3681 & 3660		7
3775		$3675-3668$	$3600-2800$	27
≈ 3775		$3695-3662$	<3600	40
3778		$3680-3675$	$3455-3450$	63
$3779-3771$	$3738-3727$	$3682-3660$	≈ 3400	29
3740		3675		19
3760		3660	$3600-2800$	61
3770		3680		53
3769				24
3774		3668		65,81
		Theoretical		
$3822-3743$	$3755-3568$	$3647-3498$		67
3778	3550	3475		84
	3750	3700		74

Terminal hydroxyls are bound directly to a single cation at oxygen lattice sites whereas the multicoordinated hydroxyls are located at low-index faces [61]. The former are able to accommodate a water molecule to hydrogen-bond on an edge or a corner site of the oxide particle while the latter are incapable of hydrogen bonding due to steric factors [61]. The assignment of multicoordinated hydroxyls to low-index faces [61] and the observed decrease in the relative amount of terminal OH species with vacuum treatment at $500-1000\,^{\circ}C$ [65] are in line with the observation that the regularity of sintered crystals is higher [39].

Based on IR spectroscopy, the tribridged OH species (at $3690-3681$ cm^{-1} and at $3670-3660$ cm^{-1}) on zirconia are

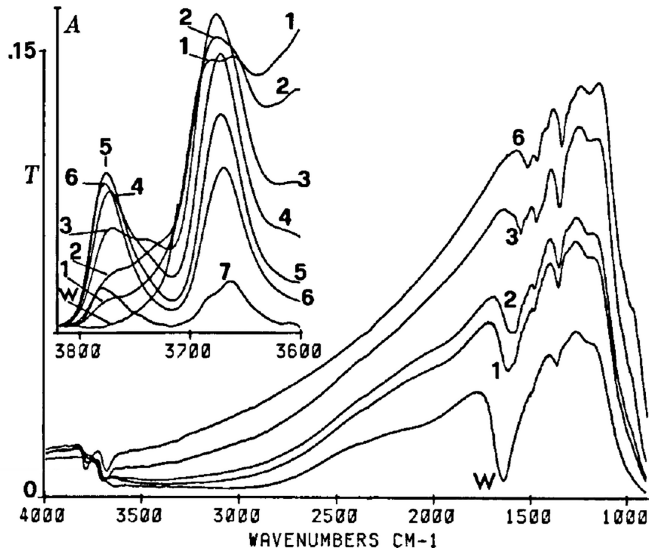

Fig. 3 The evolution of hydroxyl species with activation after rehydration. Activation conditions: W: Rehydrated sample still in 4 torr H_2O, 1: 27 °C, 5 min, 2: 27 °C, 30 min, 3: 137 °C, 30 min, 4: 247 °C, 5: 327 °C, 6: 397 °C, 7: 497 °C. Reproduced from ref. [18] with permission. Copyright 1988, Elsevier.

suggested to be actually two species [7,40], and signs of multiple tribridged species are also seen both at high [18,28] and low [18] degrees of hydration. The OH species differ slightly in their acidic character [40] and their behavior with calcination at $600-900\,^{\circ}C$ suggests that the low-frequency band ($3670-3660$ cm^{-1}) should be assigned to tribridged species at crystallographic defects selectively annealed during sintering [40]. However, in our recent investigations for reduced zirconia with no visible H-bonding effect, both terminal and multicoordinated bands shift down in wavenumber with increasing temperature [28].

The nature of the multicoordinated OH species has also been considered at the atomic level. The $ZrO_2(111)$ surface is suggested to have too small a distance between the c.u.s. O^{2-} and the c.u.s. Zr^{4+} site (only 2 Å) [40], that is not enough space to dissociate a water molecule to form terminal and bibridged OH groups. The corresponding distance between Zr^{4+} and tribridged oxygen is ≈ 2.3 Å, allowing formation of a terminal and a tribridged hydroxyl *via* dissociation [40]. Based on theory, both bibridged and tribridged species exist [67,74], Korhonen *et al.* report that at low coverages ($\theta = 0.25$ ML), there are only bibridged hydroxyls on the $(\bar{1}11)$ and $(\bar{1}01)$ surfaces [67]. Bibridged hydroxyls are also claimed to form following dissociative adsorption on the (001) surface until a full coverage ($\theta = 1$ ML) is obtained [85].

The hydroxyl IR vibrations have been determined computationally [67,74,84] as shown in Table 2. It demonstrates the large variation of calculated frequencies which span, *e.g.*, over 200

Catalysis Science & Technology Accepted Manuscript

wavenumbers for tribridged OH species. Diversity of calculated frequencies for adsorbed OH is not unique to ZrO_2 but also reported on CeO_2 [86]. The overall discrepancy between calculated and experimental frequencies can follow from three different origins. First, frequencies are typically calculated using a so-called harmonic approximation, which specifically leaves out possible anharmonic effects leading, in part, to errors in calculated frequencies. Secondly, discrepancies can also originate from the inability of density functional theory (DFT) to reliably describe the electronic structure of a given system. Thirdly, for polycrystalline oxide nanostructures, the discrepancy of calculated frequencies compared to the experimental ones can stem from the fact that an active surface site cannot experimentally be identified definitely. This may lead to an inaccurate computational adsorption site model, which differs from the real adsorption site. Moreover, the application of a cluster model to simulate ZrO_2 surfaces can impact on the calculated frequencies.

Hydroxyl densities can be estimated based on the amount of water removed from zirconia [34], water adsorbed on zirconia [27,69], or on quantification *via* ^{1}H MAS NMR [68], and these estimates are presented in Table 3. In the table, the scaled values represent OH density regardless whether it has been measured directly or by water adsorption (each water molecule is assumed to form two surface hydroxyls).

The observed amount of adsorbed water decreases with increasing temperature, as expected. Based on an estimated number of Zr atoms on the ZrO_2 surface (*ca.* 12 μmol/m^2) and water adsorption leading to formation of two OH groups, one on Zr cation and one on a surface oxygen, the estimated hydroxyl densities seem reasonable in magnitude. Nawrocki *et al.* report a theoretical maximum OH concentration of *ca.* 25 μmol/m^2 based on the average surface Zr concentration of *ca.* 12.2 μmol/m^2 [37]. The amount of induced hydroxyls (20.2 μmol/m^2 desorbed above 200 °C) [34] seems to be in agreement with the estimated total OH capacity, also Piskorz *et al.* [77] have reported similar theoretical OH site densities.

The energetics of water adsorption have been investigated both with an experimental and a theoretical approach. Piskorz *et al.* have studied the effect of surface hydration on the stability of the crystal planes using DFT calculations [77]. A hydroxylated surface is favored over the clean surface on very small crystallites ($<$ 20 Å), whereas hydration does not enhance the stability of the surface on crystallites between 500 Å and 2000 Å, and the authors claim that the transformation from clean to hydrated surface is attenuated [77]. However, this is not in line with experimental observations suggesting the hydroxylated surface to be the prevalent one. Based on microcalorimetry, the integral enthalpy of adsorption for a half-layer coverage of water (3.65 μmol/m^2) is -142 kJ/mol on monoclinic ZrO_2 nanoparticles (crystal size $100-500$ Å, specific surface area $1.6-27.2$ m^2/g) [31]. This is in agreement with the values measured for powder zirconias ($1.0-1.6$ m^2/g) [32] giving a range from -110 kJ/mol to -170 kJ/mol. Theoretical adsorption energy values typically range from -80 kJ/mol to -190 kJ/mol on (001), ($\bar{1}$11), (111), and ($\bar{1}$01) [67,69,85]. We have recently reported dissociative adsorption energies for the first adsorbing water molecule ranging from $-106\ldots-119$ kJ/mol up to -297 kJ/mol, for flat, stepped and corner adsorption sites [28]. The calculated values demonstrate the structure sensitivity of dissociative adsorption of water, which is clearly most favorable on a c.u.s. site such as a corner site suggested by our DFT calculations [28].

3.2 Manipulation of hydroxyl species

The intensity ratio of terminal and multicoordinated hydroxyls varies according to temperature, used atmosphere and pretreatment. Hydroxyl species can be added to the surface with water or hydrogen treatments and removed using heat together with inert gas or evacuation. The initial state of zirconia can usually be restored with evacuation or flushing with inert at the same temperature as before rehydration [28,53].

Sample hydration is typically carried out by adsorbing water vapor, either by letting the sample adsorb moisture from air (virgin material in [18]), equilibrating in a closed vessel with water vapor in nitrogen (to avoid CO_2 adsorption) [34], or by feeding water vapor to the sample [18,23,28,58,65]. The rehydrated sample can be used as such or after further dehydration with vacuum and/or elevated temperature (*e.g.* [18,65]). Rehydration has also been carried out by exposing the sample to hydrogen at room temperature [53] or by contacting the zirconia sample with water-saturated hydrogen for 10 min at 50 °C [42]. Unfortunately, rehydration is often described vaguely, omitting time, water vapor concentration or temperature, all relevant in controlling the degree of hydroxylation.

Commonly used methods for dehydration are vacuuming [20,24,33,70] or flushing [67] at elevated temperatures. Undissociated water adsorbed at room temperature is completely removed in vacuum by 127 °C [27] and after evacuation at 200 °C only two distinct OH bands at *ca.* 3775 cm^{-1} and 3665 cm^{-1} remain [40]. Köck *et al.* pretreated the zirconia in air at 900 °C to completely dehydroxylate the sample, and only very weak OH bands remained [62]. Evacuation at 500 °C is reported to be insufficient for complete dehydroxylation [20], but already at 550 °C spectra with no trace of surface hydroxyls after evacuation are shown [53]. The conditions necessary for total OH removal are at *ca.* $550-750$ °C *in vacuo* [18,44,65], in agreement with the enthalpies for water adsorption discussed earlier in this paper in Section 3.1. As most pretreatments and processes do not reach these conditions, the presence of these OH groups on the zirconia surface in process conditions is practically inevitable, especially in biomass-based processes, where water is present.

Catalysis Science & Technology Accepted Manuscript

This journal is © The Royal Society of Chemistry [year]

Table 3 Hydroxyl densities reported in literature

Measurement	As reported	Scaled to μmol OH/m^2	Ref.
OH concentration ($SA = 19$ m^2/g)	6.2 OH/nm^2	10.30	25
OH concentration ($SA = 110$ m^2/g)	9.4 OH/nm^2	15.61	25
Induced hydroxyls (desorbed above 200 °C) after 48h in humid N_2 at RT	20.2 μmol OH/m^2	20.2	34
OH coverage calc. from H_2 evolution after standardization (400 °C, O_2, 1h)	$2.1 \cdot 10^{13}$ OH/cm^2	0.35	20
Estimated full OH coverage before standardization	$7.2 \cdot 10^{13}$ OH/cm^2	1.2	20
Estimated chemisorption capacity at 25 °C	5.7 mg H_2O/g	26.7	33
Irreversibly adsorbed water at 25 °C	4.8 mg H_2O/g	22.5	33
Surface hydrogen after H_2O adsorption at 200 °C	4.20 H/nm^2	6.97	69
Surface hydrogen after H_2O adsorption at 300 °C	3.62 H/nm^2	6.01	69
Surface hydrogen after H_2O adsorption at 400 °C	3.22 H/nm^2	5.51	69
Full coverage of water (2x half-layer coverage)	4.4 H_2O/nm^2	14.6	31
Theoretical H_2O adsorption capacity at $\theta = 1$ ML on $(\bar{1}11)$ surface	8.9 H_2O/nm^2	29.6	77
Theoretical H_2O adsorption capacity at $\theta = 1$ ML on (111) surface	7.1 H_2O/nm^2	23.6	77
Theoretical H_2O adsorption capacity at $\theta = 1$ ML on (011) surface	5.2 H_2O/nm^2	17.3	77
Theoretical H_2O adsorption capacity at $\theta = 1$ ML on (001) surface	7.5 H_2O/nm^2	24.9	77

The partial dehydration method[18,44,53,65] can be used to vary the concentration of several types of OH groups on zirconia. Depending whether the amount of adsorbed water results from dehydration or rehydration, the surface species distribution might be different as demonstrated by Bolis *et al.*[27] by heating the sample in a closed vessel and analyzing the OH distribution on the sample before and after. Based on their findings, dehydration is systematic even in terms of the surface effects whereas rehydration is more blotchy as the water collides and dissociates on the surface as hydrogen-bonded pairs[27]. Thus allowing the system to approach equilibrium leads to a more even surface distribution. All in all, the method chosen to adjust the amount of hydroxyls influences their distribution on the zirconia surface.

Cerrato *et al.* suggest based on theory that water dissociates forming a tribridged OH at a tricoordinated c.u.s. oxygen and a terminal OH on a c.u.s. cation, leaving a c.u.s. monocoordinated oxygen in the same sphere unsaturated[40]. The presence of the suggested c.u.s. monocoordinated oxygen is in agreement with CO_2 adsorption experiments on a fully hydrated surface, yielding monodentate and bidentate carbonate species requiring the presence of basic, c.u.s. oxygen ions[40].

Based on theory, dissociative adsorption for the first adsorbed water molecule of a unit cell ($\theta = 0 \ldots 0.25$ ML) has been reported on $(\bar{1}11)$[67,77], $(\bar{1}01)$[67], and (111)[77] surfaces. The second H_2O molecule adsorbs molecularly on $(\bar{1}11)$[67,77] and (111)[77], and dissociatively on $(\bar{1}01)$[67] surfaces. The additional H_2O molecules adsorb molecularly[67,77]. For both $(\bar{1}11)$ and $(\bar{1}01)$ surfaces already the first water molecule forming two hydroxyls is hydrogen-bonded[67]. Iskandarova *et al.* have reported both dissociative and molecular adsorption enthalpies resulting in coverages of 0.5 ML and 1 ML on a (001) surface, the dissociative adsorption is favored by $45 - 75$ kJ/mol in both cases[85]. Our recent investigations suggest that at $\theta = 0.25$ ML, there is hydrogen bonding between the hydroxyl groups on the $(\bar{1}11)$ surface but not on the hydroxylated $(\bar{2}12)$ edge and corner sites[28]. Cerrato *et al.* point out that the hydrogen bonding at high hydroxyl coverages only takes place between OH species and coordinated undissociated water whereas hydrogen bonding between OH pairs is unlikely[40].

Morterra *et al.* hypothesize that if all surface oxygens on a (111) surface are transformed into hydroxyls to maintain electrical neutrality, and then dehydration takes place *via* desorbing terminal hydroxyls and hydrogen atoms from bridging OH groups (shown in Fig. 4), only bridging oxygens are left behind, and thus highly uncoordinated Zr^{4+} sites are achieved[39]. The intensity of the terminal hydroxyl species decreases more than that of the multicoordinated OH when the zirconia sample is thermoevacuated at $500 - 600$ °C after calcination at 600 °C[70]. Dehydration in vacuum at $500 - 1000$ °C followed by hydration caused the relative amount of terminal OH to decrease significantly compared to multicoordinated OH, whereas oxygen treatment ($500 - 750$ °C) before hydration had the opposite effect[65]. The decrease in terminal hydroxyls with high-temperature vacuum treatment is assigned to increasing amount of tetragonal zirconia, as the tetragonal phase is stabilized by oxygen vacancies[65].

One approach to hydroxyl studies is to replace hydrogen with its heavier isotope deuterium using D_2 or D_2O, or to replace ^{16}O with ^{18}O, all of which are easily observable in both IR and mass spectrometry. OD groups, known as deuteroxyls, have been investigated by many groups[19,21,24,42,44,56,59,61,87] while oxygen-labeling studies are more scarce[66,69,81].

Observed deuteroxyl IR wavenumbers are collected in Table 4. Erkelens *et al.* report that the ratios of the frequen-

Catalysis Science & Technology Accepted Manuscript

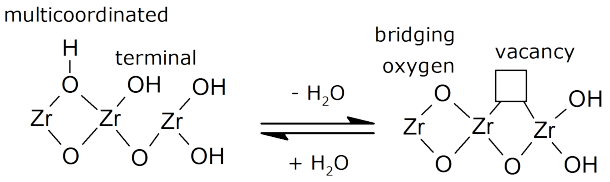

Fig. 4 (De)hydroxylation mechanism.

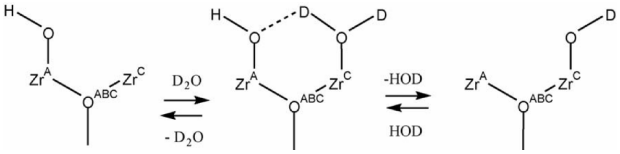

Fig. 6 The OD exchange mechanism proposed by Ignatchenko *et al.*[69]. Reproduced from ref.[69] with permission. Copyright 2006, Elsevier.

cies between the OH bands (3732 cm^{-1}, 3660 cm^{-1}, and 3584 cm^{-1}) and the OD bands (2758 cm^{-1}, 2702 cm^{-1}, and 2651 cm^{-1}) are *ca.* 1.36, in agreement with the expected isotopic substitution[56]. Similar results with additional OH band at $3738-3727\ cm^{-1}$ (OD at $2757-2748\ cm^{-1}$) were reported also by Guglielminotti[29]. A spectrum showing the changes in OH/OD groups is shown in Fig. 5.

Table 4 Experimentally determined ν(OD) wavenumbers

Terminal cm^{-1}	Multicoordinated cm^{-1}	Other cm^{-1}	Ref.
2780	2703		44
2758	2702	2651	56
2770	2695		61
2785 – 2779	2713 – 2701	2757 – 2748	29
2780	2710		59
2783	2713 – 2710		63
2760	2706		48
2760	2710		19
2782	2705		81

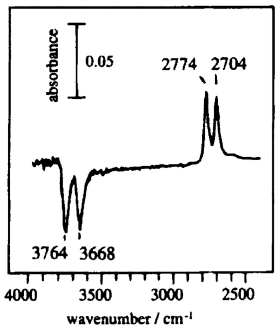

Fig. 5 Difference spectra of OH/OD species before and after 30 min in 100 torr D_2 at 150 °C. Reproduced from ref.[87].

Repeated treatments with, *e.g.*, 10 torr of D_2O vapor[44] at room temperature almost completely replace hydrogen with deuterium in both terminal and multicoordinated OH, resulting in corresponding OD groups[19,24,44,56,59,61]. The terminal species seem to exchange more easily than the multicoordinated species[24,59].

Ignatchenko *et al.* propose that the hydrogen–deuterium exchange mechanism would proceed *via* hydroxyl/deuteroxyl exchange so that a deuterated water adsorbs adjacent to an existing terminal hydroxyl species and a hydrogen bond is formed between the D_2O and the OH species[69]. Then the hydrogen-bonding deuterium atom and the original OH group desorb as HDO species, leaving the OD species on the surface. The mechanism is shown in Fig. 6.

Labeling the oxygen of water ($H_2^{18}O$) reveals that the oxygens of hydroxyls are thoroughly exchanged by 400 °C, yet at 200 °C the findings of Ignatchenko *et al.*[69] disagree with the suggested mechanism in Fig. 6. It appears that already at 200 °C the terminal hydroxyls can be exchanged but for the multicoordinated ones higher temperatures (closer to 400 °C) are required[69], and the presented mechanism should be modified to also apply for the multicoordinated hydroxyls. Based on these findings, it seems that the hydrogen scrambling follows the suggested mechanism[69] (see Fig. 6). The terminal OH species are completely exchanged *via* the normal (de)hydroxylation mechanism involving also multicoordinated OH groups and labeled $H_2^{18}O$ as deduced from the applied temperature range ($200-400$ °C). The exchange of multicoordinated hydroxyls requires a new mechanism hypothesis and we propose that multi-OH groups are removed as water, leaving behind one oxygen atom and an oxygen vacancy (see Eq. 1). This mechanism may be predominating only at high temperatures when terminal OH species have already been desorbed.

In addition to water or its deuterated counterpart, also H_2 or D_2 can be used to create surface OH or OD groups on monoclinic zirconia. He and Ekerdt have suggested that gas-phase hydrogen is able to replenish OH groups[21], the hydroxyl IR bands emerge at $200-600$ °C[9,48,53] for both terminal and multicoordinated hydroxyl species[53].

Hydroxyl formation mechanism by molecular hydrogen can be either homolytic, resulting in two hydroxyl species and two electrons[9], or heterolytic, resulting in IR-inactive Zr–H (H^+ type) species and a hydroxyl (OH) species[49]. At temperatures above 100 °C, large amounts of hydroxyl species are formed likely due to homolytic dissociation of hydrogen[48], whereas hydrogen contact at room temperature induces heterolytic dissociation[48]. Heterolytic dissociative adsorption of H_2 at room

Catalysis Science & Technology Accepted Manuscript

This journal is © The Royal Society of Chemistry [year]

temperature seems to require unhydroxylated c.u.s. Zr sites, as pretreatment above 600 °C is necessary to remove adsorbed water from the zirconia surface[26,49]. Even though Bianchi *et al.* have observed increasing hydroxyl species intensities in IR during H_2 treatment, they report no adsorption or desorption of hydrogen at $25-400$ °C, and no water evolution during H_2-TPR from 25 °C up to 700 °C[53]. Assuming no redox process concerning the Zr cations, a hydrogen desorption mechanism is postulated for Zr–H and Zr–OH sites leading to Zr and Zr–O sites, as hydrogen adsorbed at 550 °C is desorbed from m-ZrO_2 at 600 °C[9].

According to Syzgantseva *et al.*, hydrogen dissociates on Zr^{3+} with a neighboring oxygen vacancy (v_o), leading to formation of Zr–H hydrides and the transformation of Zr cations into Zr^{4+} species[82]. The proposed mechanism is presented in Fig. 7. Addition of gas-phase oxygen to the Zr–H hydrides, produced by gas-phase H_2 at room temperature, increases the OH intensity at 3668 cm^{-1} (generally considered as multicoordinated OH), creates the 3774 cm^{-1} OH band (terminal OH) and decreases the intensity of the Zr–H species at 1565 cm^{-1}[81]. Substituting regular oxygen ($^{16}O_2$) with isotopically labeled oxygen ($^{18}O_2$) does not affect the position of the OH bands (expected shift 11 cm^{-1}), thus the OH formation seems to occur on lattice oxygen rather than the gas-phase originating oxygen species[81].

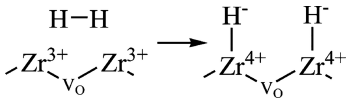

Fig. 7 The hydrogen dissociation mechanism proposed by Syzgantseva *et al.*[82]. Reproduced from ref.[82] with permission. Copyright 2012, American Chemical Society.

Treatment with deuterium gas at 200 °C (1h, 18 torr) and 250 °C (1h, 250 torr), is sufficient to exchange virtually all hydrogen of hydroxyl groups to deuterium[56]. He and Ekerdt report that the deuterium in OD groups is replaced by hydrogen already at 200 °C with hydrogen dissociating on the zirconia surface[19]. At 150 °C in 488 kPa of D_2, half of the hydrogen in surface OH species are changed to deuterium within 30 seconds[42]. The H/D exchange takes place already at 100 °C with D_2 in the gas phase, however, at 200 °C the exchange rate increases considerably[26]. The activation energies of the H/D exchange reaction with D_2 are similar for both terminal and multicoordinated hydroxyls, and they seem to increase with the progress of the reaction[26]. This is interpreted to be due to the overall exchange (migration and replacement of atomic hydrogen by deuterium) being limited by D migration on the surface, subject to heterogeneity of potential barriers to various sites[26].

Merle-Méjean *et al.* have found that on an air-calcined zirconia the hydroxyl species are H/D exchanged in contact with D_2 (507 °C, 100 hPa) so quickly that it gives reason to believe the OH species are on the surface only[63]. Conversely, on the steam-calcined zirconia there are some hydroxyls exchanged to deuterium-containing species so slowly (during several hours), if at all, that they must be elsewhere in the oxide, likely in the bulk[63].

The presence of formate species is suggested to decrease the number of available sites for H_2/D_2 dissociation as well as partially block the path for surface transport of H or D atoms[42]. If there are formates on the surface, the H/D exchange between OH and OD species at 150 °C is $4-36$ times slower depending on the formate coverage (0.3 or 0.8 times the maximum coverage)[42]. The overall extent of the H/D exchange of multicoordinated OH to OD is limited to 9% with formate and 2% with methoxy species as compared to normal ZrO_2 surface[26].

4 Interaction with CO

Upon contact with monoclinic zirconia, CO tends to form several surface species: at low temperatures up to *ca.* 100 °C the preferred species is linearly adsorbed CO, at higher temperatures the dominating surface species is formate. In addition to these, also carbonate and carboxylate-type species have been observed.

4.1 Linear CO species, formation and stability

CO adsorption at room temperature leads to the formation of linear CO species on cationic sites of the zirconia surface (see Fig. 8), the corresponding bands in IR spectra are located at *ca.* $2200-2170$ cm^{-1}[5,18,48,50]. Spectra of the linear CO species as a function of CO pressure and with two differently prepared samples are shown in Fig. 9. The presence of a weak band at 2112 cm^{-1} is reported after C adsorption at room temperature[48]. With adsorption below room temperature, *e.g.*, at $-173\ldots-195$ °C, the range of adsorbed linear CO species extends to *ca.* $2200-2140$ cm^{-1} at varying CO pressures (from 10^{-4} to 40 torr)[39,58].

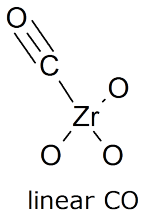

Fig. 8 Linearly adsorbed CO species.

Morterra *et al.* report that the linearly adsorbed CO species seen in IR at room temperature are at wavenumbers 2198 –

Catalysis Science & Technology Accepted Manuscript

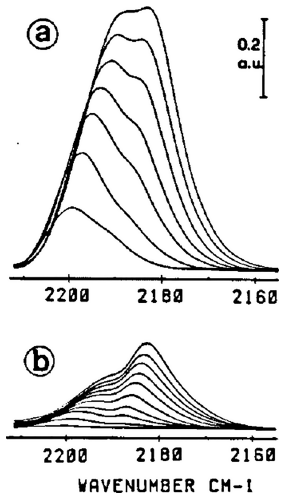

Fig. 9 CO adsorbed at room temperature on a ZrO_2 sample calcined at 597 °C (a) and at 997 °C (b), followed by vacuum-activation at 597 °C. $P_{CO} = 2 \cdot 10^{-1} \ldots 1.2 \cdot 10^{2}$ torr. Reproduced from ref. [39] with permission. Copyright 1991, Elsevier.

2187 cm^{-1} and 2188 – 2174 cm^{-1}, named $(CO)_H$ and $(CO)_L$ after the high-frequency and low-frequency bands [18]. Also Guglielminotti has adsorbed CO to zirconia at room temperature, and his results for either reduced (550 °C) or oxidized (400 – 550 °C) and vacuum-activated (400 °C) samples show strong bands at around 2200 cm^{-1} [29]. For samples reduced at 300 °C and/or vacuum-activated at 500 °C after oxidation, adsorbed CO is observed also at 2110 cm^{-1} [29].

The IR bands at *ca.* 2200 – 2190 cm^{-1} are interpreted as CO adsorbed on Zr^{4+} [6,27,29] and the band at *ca.* 2120 – 2110 cm^{-1} is assigned to CO on Zr^{3+} surface ions [6,7,9,29,81], whereas ESR (electron spin resonance spectroscopy) results are interpreted so that Zr^{3+} surface ions do not interact with CO at room temperature [47]. The appearance of IR bands assigned to adsorbed CO at higher wavenumbers than gas-phase CO (at 2202 cm^{-1}) is attributed to polarization of the CO molecule on the surface [48]. At room temperature the OH groups are not modified during CO adsorption [54].

The $(CO)_H$ and $(CO)_L$ species are suggested to be on two types of Lewis-acidic centers [18], both types assigned as Zr^{4+} ions [27]. For CO chemisorption, these centers are suggested to be caused by differences in crystallography and/or coordinative configurations as the $(CO)_L$ intensity increases while the $(CO)_H$ intensity declines with increasing activation temperature as a result of the beginning sintering process [18]. The $(CO)_L$ sites are therefore assigned to flat sites whereas the $(CO)_H$ sites are thought to be on rougher (high-index) planes or structural defects: steps, kinks, or corners [27]. Sintering the surface indeed causes a sharp relative decline on $(CO)_H$ intensity (at *ca.* 2190 cm^{-1}) in IR, and the sintered surface seems to have more extended and regular flat surface sites based on HRTEM images [39].

Linear CO is reversibly adsorbed on the surface at room temperature as removing the CO from gas phase results in the disappearance of its IR band [20,27,54,55]. CO adsorption at room temperature at constant CO pressure shows constant intensity against time on stream if measured by the band at *ca.* 2192 cm^{-1} [20,54], indicating unactivated adsorption. Jung and Bell present an interesting scheme (see Fig. 10) relating linearly adsorbed CO and its interactions with the zirconia surface [25]. In the scheme they show two differently coordinated adsorbed CO molecules with bicarbonate and bidentate carbonate as transformation intermediates: in the former case the Zr^{4+} cation will have a lower Lewis acidity in the vicinity of an OH group, leading to a lower displacement value of the IR wavenumber compared to the gas-phase CO IR band than with the bidentate carbonate intermediate in a c.u.s. oxygen environment [25].

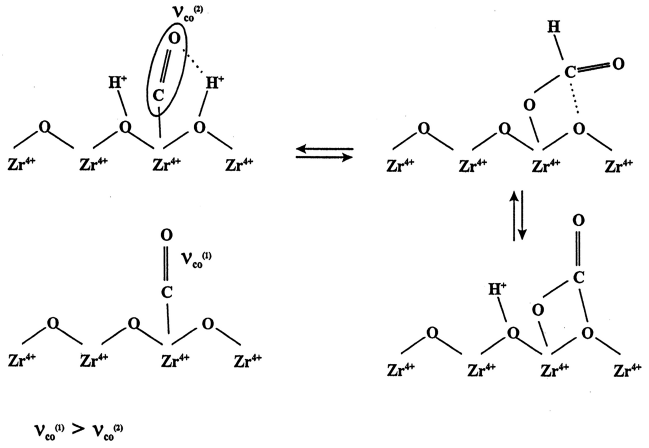

Fig. 10 Interactions of linearly adsorbed CO with the ZrO_2 surface. Reproduced from ref. [25] with permission. Copyright 2000, Elsevier.

Increasing the CO partial pressure increases the adsorbed CO band intensity [20,52]. The intensity ratio for the two adsorbed CO species favors $(CO)_H$ at low coverages and $(CO)_L$ at high CO pressures [18,27]. An increase in the CO partial pressure shifts the IR band position down from *ca.* 2195 cm^{-1} to 2188 cm^{-1} [27,50,52,54], and the overall surface area of the band indicates adsorption according to Langmuir's adsorption model with increasing CO partial pressure [54].

Increasing the adsorption temperature shifts the main band at *ca.* 2190 cm^{-1} towards higher wavenumbers [18,55]. This shift is attributed to inductive effects, as the charge-release mechanism of the adsorbed CO is affected by those, as well as the influence of other surface species (*e.g.* OH) on the adsorbed CO [18]. The temperature range with detectable linear CO bands extends typically to *ca.* 100 – 150 °C [48,54,55], but it has been reported even at 250 °C [25] at 2184.9 cm^{-1} (CO pressure not

Catalysis Science & Technology Accepted Manuscript

This journal is © The Royal Society of Chemistry [year]

reported). Ma *et al.* observed a band at 2109 cm^{-1} during CO adsorption at 350 °C, linked to CO adsorption on c.u.s. Zr^{3+} [7].

The reported linear CO coverages are scaled to μmol/m^2 and collected in Table 5. The amount of adsorbed CO depends on the adsorption temperature, the coverage at −173 °C is significantly higher than the coverage at room temperature. As can be seen in Table 5, dehydroxylation increases the linear CO adsorption capacity [20], as dehydroxylated surfaces have a higher number of bare zirconium cations. Increasing activation temperature results in increasing monolayer capacities for both $(CO)_L$ and $(CO)_H$ [27], as expected due to lower hydroxyl coverage with increasing activation temperature. It has been estimated that 50% of the dehydroxylated sites can adsorb CO reversibly [20]. The capacity for the $(CO)_H$ species is significantly lower than for the $(CO)_L$ species, the latter almost fourfold compared to the former [27].

Dulaurent and Bianchi have assumed Langmuir adsorption, calculated adsorption coefficients from IR data and used them with statistical thermodynamics to extract heats of adsorption, and their results range from 55 kJ/mol to 42 kJ/mol (at zero and saturation coverage, respectively) [55]. Molar heat of adsorption determined with microcalorimetry is reported to be $65-73\pm2$ kJ/mol for $(CO)_H$ and $44-50\pm2$ kJ/mol for $(CO)_L$ [27], and for Lewis-acidic sites at vanishing coverages *ca.* 60 kJ/mol. Based on theory, the adsorption energy of linearly adsorbed CO was determined to be −45 kJ/mol [28]. To give an idea of the strength of the CO adsorption on the Zr^{3+} sites, CO on Zr^{4+} (at *ca.* 2200 cm^{-1}) can be removed by evacuation at room temperature and CO on Zr^{3+} (at *ca.* 2110 cm^{-1}) is slightly more strongly bound to the zirconia surface, yet also possible to evacuate at room temperature [29]. The observed IR band intensities of the $(CO)_H$ and $(CO)_L$ species with increasing CO pressures are in line with their heats of adsorption: the $(CO)_H$ with a higher heat of adsorption has a higher intensity at low pressures and and *vice versa* at higher pressures [27].

As shown in Table 5, the linear CO adsorption capacity on dehydroxylated surfaces is higher than on hydroxylated surfaces. The hydroxyl species has an adverse effect on CO adsorption as linear CO [20,27,28], completely suppressing CO adsorption at room temperature already at a surface concentration of 2.4 μmol/m^2 H_2O [27], corresponding to a 20% surface coverage. The more strongly adsorbed linear CO species, $(CO)_H$, seems to be suppressed more than the more weakly adsorbed species when the sample is changed from a dehydroxylated one to one with a low OH coverage [27], suggesting that the site for $(CO)_H$ is the preferred site for hydroxyl formation. Four irreversibly held water molecules are required to eliminate one acidic site based on adsorption capacity experiments at varying degrees of hydration [27]. This 4:1 ratio between water and CO suggests that adsorption sites for linearly adsorbed CO represent only a minority of the sites available for water adsorption. This division is also reflected in the adsorbed amounts of water or OH groups (Table 3) and linearly adsorbed CO (Table 5).

In addition to increasing the adsorption capacities, dehydroxylation seems to shift the bands of the adsorbed CO species up in wavenumber, once full dehydroxylation has been carried out by evacuation at 597 °C, the bands only decrease in intensity: especially the $(CO)_H$ band intensity decreases as is expected due to the sintering process first affecting the minority sites [27]. Morterra *et al.* indicate that on a highly hydrated surface, local interactions among hydroxyls exceed the adsorbate-adsorbate interactions caused by CO, *i.e.*, the ordered CO oscillator network is interfered with the hydroxyls present [39].

Morterra *et al.* have looked at CO adsorption to cationic Zr sites after rehydration and they report that the CO species adsorbing at 2145 cm^{-1} (assigned to CO adsorbed to Zr^{4+} centers *via* a σ bond) are quickly suppressed with water, but the lower wavenumber band tends to downshift from 2112 cm^{-1} to 2102 cm^{-1} (proposed to be c.u.s. cationic center Zr^{n+}, where $n<4$) and increase in intensity [8]. The overall surface coverage of charge-releasing CO species inductively affect also the position of the adsorbed CO band [8].

Even though hydroxylation decreases the linear CO adsorption capacity [27,58], surface hydroxyls are an important surface site for CO adsorption as formate species [5,21]. Linearly adsorbed CO intensities during room-temperature adsorption have been compared before and after CO adsorption at elevated temperature [54,55]. Dulaurent and Bianchi report that after CO adsorption at 85 °C or 152 °C, cooling to 27 °C and another CO adsorption, the absorbance of the linear CO band is reported to decrease by 12% or 35%, respectively [55]. Mugniery *et al.* show spectra where formate preadsorption at 300 °C shifts the linear CO bands from 2192 cm^{-1} to 2177 cm^{-1} [54]. When these bands are compared to the spectra of Morterra *et al.* [38] we note that the $(CO)_H$ species is suppressed by formates, linking the formate and the $(CO)_H$ to the same Zr^{4+} surface site. As mentioned earlier, when investigating the CO pressure effect on the band, $(CO)_L$ is the preferred species at high coverages. However, it is not clear whether that applies also to the increasing formate coverage (or coverage of any species) or if the $(CO)_H$ site is occupied or otherwise hindered due to the adsorbed formate species.

4.2 Formates, formation and decomposition

Formate species consists of a $HCOO^-$ unit connected to a surface zirconium cation from oxygen atom(s). Two different surface configurations have been proposed for the formate species: a bidentate formate [20,22,30,42] and a monodentate formate [22,42] shown in Fig. 11. Main IR bands of formate species on monoclinic zirconia are observed typically (see Fig. 12) at *ca.* 2965 cm^{-1}, 2880 cm^{-1}, 1565 cm^{-1}, 1387 cm^{-1},

Catalysis Science & Technology Accepted Manuscript

Table 5 Linear CO coverages reported in literature

Measurement	As reported	Scaled to μmol/m^2	T_{ads}	P_{CO}	Ref.
Adsorbed quantities of CO [a]	up to 220 μmol/g	up to 2.7	RT	N/A	50
Monolayer (ML) capacity for $(CO)_H$	0.12 – 0.24 molec./nm^2	0.2 – 0.4	RT	70 or 20 torr [b]	27
Monolayer (ML) capacity for $(CO)_L$	0.5 – 0.8 molec./nm^2	0.8 – 1.3	RT	N/A [c]	27
Monolayer coverage for CO	0.65 CO sites/nm^2	1.1	RT	60 torr	52
ML capacity for fully dehydroxylated sample	1.04 molec./nm^2	1.73	RT	N/A	27
$Zr^{+\delta}$ sites available for linear CO adsorption	$8 \cdot 10^{13}$ sites/cm^2	1.33	RT	N/A	55
Total CO coverage on a hydroxylated surface	2.7 molec./nm^2	4.5	−173 °C	260 Pa	58
Total CO coverage on a dehydroxylated surface	3.8 molec./nm^2	6.3	−173 °C	260 Pa	58

[a] Assuming full adsorption on the surface from fed known amount of CO. IR band in the presence of CO gas at 800 Pa is thrice as intensive as the one with 2.7 μmol/m^2.
[b] Saturation pressure, 70 torr for samples activated at 397 °C and 597 °C, 20 torr for sample activated at 797 °C.
[c] Estimated to be 30% higher than adsorption capacity at 130 torr.

1379 cm^{-1} and *ca.* 1365 cm^{-1} [5,19,22,23,88], listed with their originating vibrations as well as thoretical IR bands in Table 6. Unlike for the linearly adsorbed CO species, formate formation (see Eq. 2) is an activated process, and its rate expression is shown in Eq. 3.

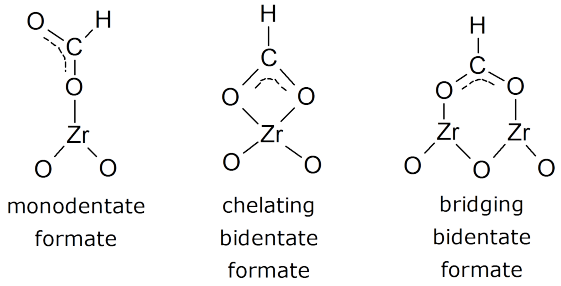

Fig. 11 Monodentate and bidentate formate species.

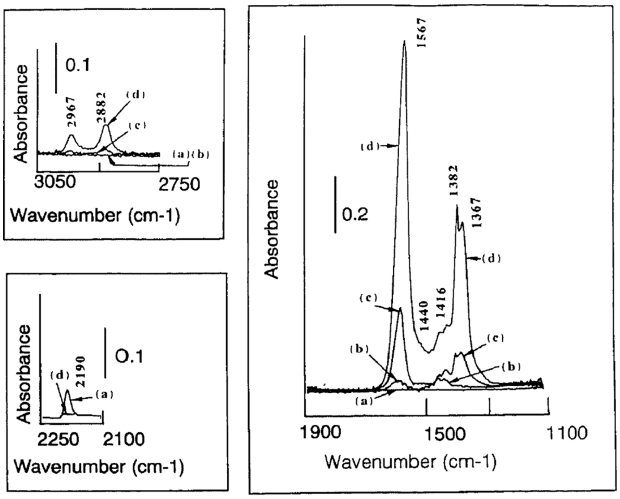

Fig. 12 Formate and linear CO spectra at (a) 25 °C, (b) 150 °C, (c) 250 °C, and (d) 350 °C in 5% CO/He. Reprinted from ref. [20] with permission. Copyright 1993, Elsevier.

$$CO + OH* \leftrightarrow COOH* \quad (2)$$

$$r_f = k \cdot P_{CO} \cdot [OH*] \quad (3)$$

Due to the activated formation process, at low temperatures (*e.g.* $T < 200$ °C) the adsorption time affects the amount of formate formed, whereas at high temperatures the system quickly reaches equilibrium, however, the equilibrium coverage is also temperature-dependent. The activated nature of the process is demonstrated with increasing intensity of the formate IR bands at different temperatures (25 – 350 °C) with adsorption times ranging from 30 min up to 18 h [19,42,54]. Formate formation requires rearrangement of at least three bonds, the cleavage of the O–H bond, and the formation of the O–C and the C–H bonds [28]. The theory-based estimate for the activation energy of formate formation is 154 kJ/mol [28], which is in agreement with the experimental observations, yet no experimental value for the activation energy has been reported.

Overall the temperature range of formate observations is wide, ranging from *ca.* 85 °C up to 550 °C [7,20,24,25,28,48,55]. The formate intensity maximum is at *ca.* 300 – 400 °C [23,28], depending on the pretreatment and measurement conditions, with increasing intensities reported at lower temperatures [48]. All in all, the formate coverage depends on the adsorption conditions (temperature, CO pressure) and the contact time with CO. With increasing temperature (240 – 400 °C) the formate coverage decreases [23] while formate intensity increases with increasing CO concentration in the gas phase [23]. Silver *et al.* have adsorbed CO on pure ZrO_2 at 500 °C and they only discovered formates on the surface, no (bi)carbonates or adsorbed CO species [45].

Catalysis Science & Technology Accepted Manuscript

This journal is © The Royal Society of Chemistry [year]

Table 6 Experimentally and theoretically[a] determined formate wavenumbers

Conditions p_{CO}, T_{ads}	ν_{as}(COO)+ν_s(COO) cm^{-1}	ν(CH) cm^{-1}	ν_s(COO)+δ(CH) cm^{-1}	ν_{as}(COO) cm^{-1}	δ(CH) cm^{-1}	ν_s(COO) cm^{-1}	Ref.
Experimental							
1 – 60 torr CO, 25 °C	2950 – 2850		-	1610 – 1580	1400 – 1350		5
100%, 25 – 500 °C	2950[b]	2880	-	1580	1390	1360	19
100%, 400 °C	-[c]	-[c]	-	1575/1530	1386	1361	24
5% CO, 25 – 350 °C	2967	2882	2740	1567	1382	1367	20
162 kPa CO, 250 °C	2965	2881	-	1568 – 1550	1385	1370	42
4% CO, 25/250 °C	≈2970	≈2880	-	1570	1380	1365	30
100% CO, 350 °C	2973/2968	2889/2880		1570/1563	1390/1380	1361/1360	7
5%, 30 – 580 °C	2964	2881	2747	1564	1384	1365	22
8 – 65% CO, 240 – 400 °C	2969	2886	-	1560	1384	1371	23
5% CO, 100 – 550 °C	2960	3870	2755/2730	1568 – 1567	1386 – 1385	1367	28
Theoretical							
Bidentate to 2 Zr, ($\bar{1}$11)	2915	2974	2754	1555	1394	1360	22
Bidentate to 1 Zr, ($\bar{1}$11)	2845	2997	2676	1544	1375	1301	22
Bidentate to Zr and O, ($\bar{1}$11)	2765	3138	2504	1585	1324	1180	22
Monodentate, ($\bar{1}$11)	2843	2892	2473	1717	1347	1126	22
Bridging bidentate, ($\bar{1}$11)	2914	2929	2773	1561	1420	1353	28
Bridging bidentate, ($\bar{2}$12)	2901	2918	2721	1565	1385	1336	28
Bridging bid., ($\bar{2}$12) corner	2860	2957	2694	1534	1368	1326	28

[a] Combination modes (ν_{as}(COO)+ν_s(COO)and ν_s(COO)+δ(CH)) for theory-based vibrations were obtained as a sum of the corresponding frequencies.
[b] The band not originally assigned as formate band rather as methoxide.
[c] The author states that the "absorption in the 3000 cm^{-1} region is very weak", a band near 2900 cm^{-1} is discernable in the spectrum.

At 250 °C the monodentate formate has a maximum at 1589 cm^{-1} and bidentate formate has maxima at 1568 cm^{-1}, 1388 cm^{-1} and 1371 cm^{-1} [42]. The authors also suggest that the formation of monodentate formate is intensified with increasing time in contact with CO, in agreement with activated formation process, and that the shift from bidentate to monodentate formates is due to repulsion among the bidentate formates at high surface concentrations [42] as shown with increasing time-on-stream (CO at 250 °C) at 1568 cm^{-1} separating into two bands at 1589 cm^{-1} and 1556 cm^{-1}.

According to Bianchi *et al.*, the formate species would be probably a bidentate as the difference between the observed bands at 1567 cm^{-1} (ν_{as}(OCO)) and 1367 cm^{-1} (ν_s(OCO)) is 200 cm^{-1} [20], and the same deduction has been used by Ma *et al.* for formate bands at 1570 cm^{-1} and 1361 cm^{-1} [7], both assigning the species based on the band separation. For carbonates, the typical difference should be *ca.* 100 cm^{-1} in the monodentate case and 300 cm^{-1} in the bidentate case [89]. Bianchi *et al.* also state that another formate species might cause the band at 1382 cm^{-1}; however, it should also have a doublet band near 1570 cm^{-1}, close to the one of the bidentate formate [20].

Korhonen *et al.* have suggested a reaction scheme where the bidentate formate formation proceeds *via* an activated monodentate complex [22]. They state that based on DFT calculations the formate is likely in a bidentate configuration as the monodentate is unlikely to be stable [22]. Our investigations indicate a bridging bidentate formate configuration as the most stable geometry on all the tested surfaces [28].

Formate forms on a surface hydroxyl species. Pozdnyakov and Filimonov stated already in 1972 that the formate is formed due to CO reacting with the surface hydroxyls [5]. Yamaguchi *et al.* in 1978 have shown formation of formate and disappearance of terminal OH and multicoordinated OH bands following the adsorption of deuterated acetone-d_6, the terminal OH being more reactive toward formates than the multicoordinated one [59]. Amount of formate formed is dependent on the surface hydroxyls, a decrease in formate formation shown by Jackson and Ekerdt by removing water from CO/H_2 feed [10] and by Bianchi *et al.* by dehydroxylating the surface [20]. He and Ekerdt suggested that formate formation proceeds *via* gas-phase CO and surface OH group [21].

Formate formation has been reported at low temperatures (25 °C and 160 °C) on terminal OH (IR band at 3770 cm^{-1}) [20]. In addition to the terminal OH site, formate formation on multicoordinated OH (band at 3680 cm^{-1}) has been reported at higher temperatures (250 – 350 °C) [7,20,42]; however, some experimental [23] and theoretical [22] results do not support the par-

Catalysis Science & Technology Accepted Manuscript

ticipation of the multicoordinated OH species. Jung and Bell suggested that the primary route for formate formation is *via* gas-phase CO and an OH group, after 9 hours at 250 °C and 162 kPa CO, all terminal hydroxyl species are consumed to formate formation as well as 38% of the bridged hydroxyl species[42]. Based on their spectral evidence[42], it seems that the consumption of terminal OH species is faster than that of multicoordinated OH species, yet whether all bridged hydroxyls can be consumed is unclear based on the evidence.

Jackson and Ekerdt suggested that formate formation in methanol synthesis involves an oxygen vacancy and an adjacent bridged hydroxyl site so that there is a terminal CO intermediate, the scheme is shown in Fig. 13[10]. However, their suggestion is in contradiction with some more recent results reporting that indeed the terminal hydroxyls participate in the formate formation[23,42].

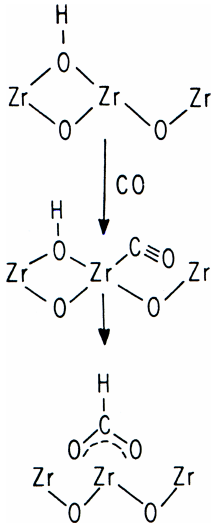

Fig. 13 Proposed formate formation mechanism as a part of methanol synthesis over ZrO_2. Adapted from ref.[10] with permission. Copyright 1986, Elsevier.

Formate decomposition has been proposed to take place by two different pathways: dehydrogenation producing CO_2 and H_2, and dehydration releasing CO and H_2O, to follow the naming of He and Ekerdt[21]. Similar decomposition pathways have been proposed by Bianchi *et al.* suggesting the release of CO and restoring the OH groups[20], and in our investigations suggesting that the dehydration is two separate reactions: first reversible formate decomposition to CO resuming surface hydroxyls and then dehydroxylation to produce H_2O, as the dehydroxylation process is observed at a similar temperature range also without CO present in the gas phase[28]. A lower limit estimate for the activation energy for the dehydrogenation reaction is its reaction energy at $178-363$ kJ/mol based on theory[28]. The typical temperature range for formate decomposition is above 300 °C[28], a desorption maximum has been reported at 410 °C[20]. The activated formate formation (increasing uptake rate up to 300 °C) and the formate decomposition pathways are demonstrated in Figure 14, where the zirconia sample is linearly heated from 100 °C to 550 °C in the presence of 2% CO, the y-axis corresponds to release/uptake from the sample.

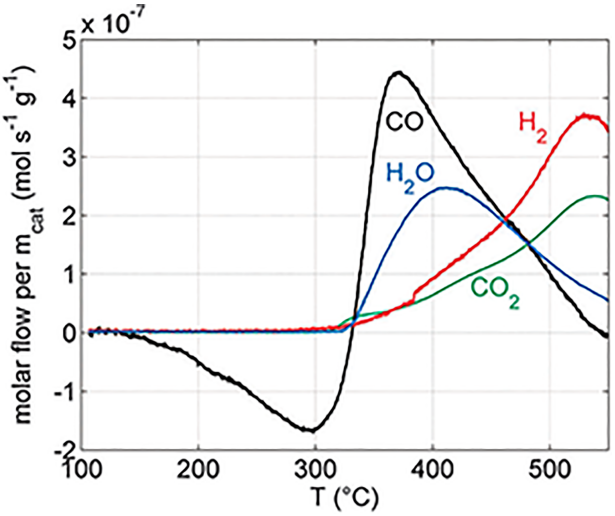

Fig. 14 Temperature-programmed surface reaction (TPSR) in the presence of CO on reduced ZrO_2. The y-axis corresponds to release (+) or uptake (-) from the sample. Reproduced from ref.[28] with permission from the PCCP Owner Societies.

Bianchi *et al.* have reported amounts of CO, CO_2 and H_2 that have adsorbed/desorbed during temperature-programmed desorption (TPD) after CO adsorption[20]. Not all carbon species are recovered, suggesting that the surface is not empty of formate (*ca.* 10% of the CO adsorbed at 350 °C unaccounted for) by the end of the desorption process with T_{max} at 410 °C[20]. Based on the observed CO_2/H ratio the surface species is claimed to be formate[20]. The decomposition routes of formate have been reported to be either completely reversible decomposition resulting in restoring the terminal hydroxyls[23] or that only about $20\ldots40$% of formate decompose forming hydrogen while the rest is decomposed reversibly[20,28]. For ceria-based catalysts, the presence of co-adsorbed water on the catalyst significantly increased the decomposition rate of formate to CO_2 and H_2[90,91] and the same likely applies to zirconia as well. Also Korhonen *et al.* report observations of CO_2 as formate decomposition product above 500 °C[22]. The presence of an active metal (*e.g.* platinum) increases the rate of formate decomposition to CO_2 and H_2[23], presumably by associating hydrogen (analogous to water-gas shift reaction), enabling a reasonable temperature window instead of 500 °C or more.

The adsorption temperature has a significant effect on the

Catalysis Science & Technology Accepted Manuscript

This journal is © The Royal Society of Chemistry [year]

amount of CO desorbed from the surface as CO_2 during TPD, yet the overall profile of the CO_2 desorption curve remains qualitatively similar[30]. CO desorption was clearly observable only after adsorption at 200 °C or 250 °C. At 250 °C there are formates on the surface according to IR[30], thus the CO desorption is likely due to decomposition of surface formate species and the CO_2 originates from formates or, especially after low-temperature adsorption of CO, (bi)carbonate species. The temperature of maximum desorption was in the range of 330 °C for CO_2 and $330-430$ °C for CO desorbing after CO adsorption.

Köck *et al.* have adsorbed CO on ZrO_2 from room temperature up until 600 °C, yet their pretreatment (annealing at 900 °C and thereafter oxidation at 600 °C) of the sample has quenched most of the surface hydroxyls, leaving formate formation negligible and thus supporting the formate formation mechanism based on surface hydroxyl species[62].

If CO adsorption at $85-250$ °C is followed by cooling down to 25 °C, the intensity of the linear CO band at 2190 cm^{-1} is smaller (by 12% with T_{ads} at 85 °C, 35% at 152 °C) with increasing preadsorption temperature compared to room temperature preadsorption[20,55]. This is assigned to the formation of formate species at cationic Zr sites[54] which are thought to be the sites where CO adsorbs linearly[6,18,27,29]. When combined with our observations that formate formation at 100 °C in the presence of CO in the gas phase is accompanied by decreasing linear CO intensity (see Figure 15)[28], it is suggested that site competition takes place and that linear CO facilitates formate formation compared to gas-phase CO. Assuming a bidentate formate species formed on a terminal OH and bound to a Zr cation (see Fig. 11), the cation site necessary for linear CO adsorption is blocked by the formate.

Measured adsorbed or desorbed CO amounts reported in literature are collected in Table 7. Increasing adsorbed/desorbed amounts of CO are reported with increasing adsorption temperature up to 350 °C[20,30]. Both Bianchi *et al.*[20] and Pokrovski *et al.*[30] have applied a similar TPD method, where adsorption is carried out at elevated temperature (T_{ads} in the table) followed by cooling to room temperature, and thereafter temperature-programmed heating begins. The desorbed amount of CO_x reported by Bianchi *et al.*[20] (0.12 μmol/m^2) are significantly lower than those reported by Pokrovski *et al.*[30] (0.35/1.34 μmol/m^2) after adsorption at 250 °C, while the specific surface areas are *ca.* 200 m^2/g and 19/110 m^2/g, respectively. The values reported in our recent work[28] seem to be larger than those by others; this might be explained with a different experimental procedure, where weakly bound CO is not removed from the surface prior to temperature-programming.

As mentioned previously, the terminal OH group is the active species concerning formate or bicarbonate formation on the zirconia surface after gas-phase adsorption of CO at elevated temperature ($240-400$ °C)[23]. The activity of the terminal OH group has been further investigated using isotope-labeled experiments with D_2O and D_2. When deuterated formates were formed *via* CO adsorption to OD (deuteroxyl) species, they could be transformed back to HCOO with contact to hydrogen at 200 °C[19]. H/D isotope exchange of the surface formates with gas-phase D_2 seems to be possible, yet slow and competing with formate decomposition already around 300 °C[26]. Only $2-3$% of the surface formate species are exchanged to DCOO species at 150 °C in 488 kPa D_2[42]. The necessity of gas-phase D_2 for formate scrambling was demonstrated as the H/D exchange did not proceed between formates and surface deuteroxyls[26]. However, as formates can form on surface deuteroxyls achieved by surface treatment with D_2O[19], it is implied that once formed, formates are stable and do not scramble with each other *via* cleavage of the $O_{support}$–C bond.

4.3 Other species formed during interaction with CO

In addition to linear CO and formates also other species have been observed during CO adsorption. These species reveal the diversity of the interaction between CO and monoclinic zirconia although the number of reported observations remains low. The observed species include bidentate carbonates[48], probably also carboxylate species as the band at 1416 cm^{-1} and its symmetric counterpart at 1560 cm^{-1} have been confirmed *via* difference spectra[20]. Monodentate carbonate (1469 cm^{-1}) and ion carbonate bands (1303 cm^{-1} and 1442 cm^{-1}) were observed after CO adsorption at 350 °C[7]. Similarly, ionic carbonate and carboxylate species have been suggested, their bands disappear when CO is removed from the gas phase at 400 °C while the formate species remain intact[54]. When comparing CO adsorption at 350 °C on hydroxylated and dehydroxylated samples, the latter shows less intense formate bands but more intense bands at 1440 cm^{-1} and 1416 cm^{-1} as well as new bands at 1540 cm^{-1} and 1317 cm^{-1}, suggesting carbonates present on the surface and perhaps also carboxylate species[20]. Also bidentate carbonates have been reported form during high-temperature adsorption (above 250 °C) of CO[48]. Ma *et al.* have suggested that bicarbonate and carbonate species could be formed on ZrO_2 from CO *via* carboxylate surface species[7]. He and Ekerdt have suggested that CO is adsorbed on the metal oxide oxygen forming a [COO] intermediate and then reacting further to carbonate or formate[21]. All these species require the participation of one or two surface oxygen atoms.

CO adsorption followed by carbonate formation and CO_2 desorption leads to surface reduction as oxygen is removed from the surface. During temperature-programmed surface reaction (TPSR) in CO, CO_2 amounts detected correspond to $10-14$% of surface oxygen atoms depending on pretreat-

Catalysis Science & Technology Accepted Manuscript

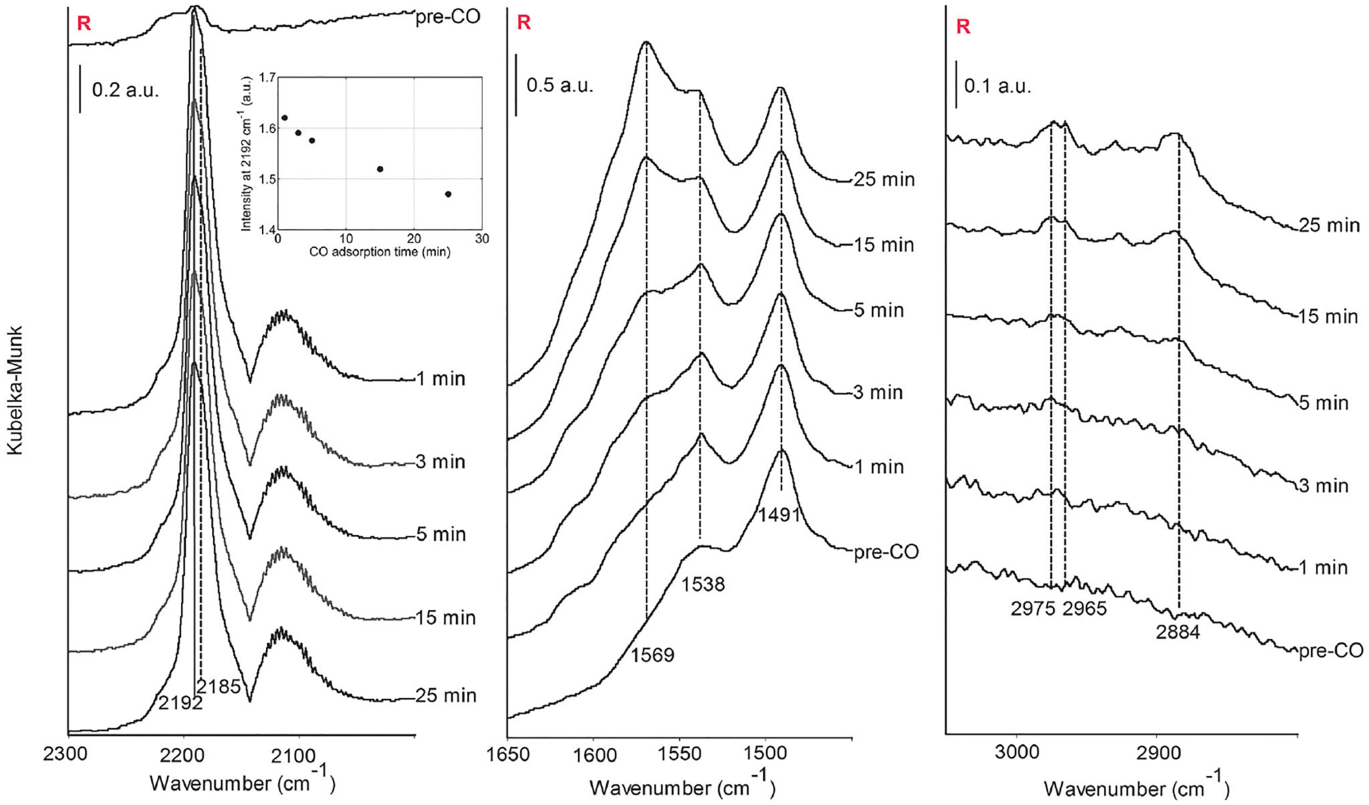

Fig. 15 Decreasing linearly adsorbed CO intensity (at $2192-2185\ cm^{-1}$) and increasing formate intensity (at $1569\ cm^{-1}$, $1538\ cm^{-1}$, $2975-2965\ cm^{-1}$ and $2884\ cm^{-1}$) with time in contact with CO at 100 °C. Reproduced from ref.[28] with permission from the PCCP Owner Societies.

ment of the zirconia[28]. Pulse oxidation experiments show that estimating the monolayer coverage based on assuming a $ZrO_2(100)$ surface, 13.6% of the surface oxygen atoms can be removed by CH_4 at 900 °C[92].

During static adsorption of CO at 200 °C and above, CO_2 formation was observed in the IR spectra, originating either from formate decomposition or from CO oxidation *via* lattice oxygen species[62]. Ionic carbonate was observed during CO adsorption at 150 °C and above on rehydrated zirconia, and it was released as CO_2 instead of CO[20].

Silver *et al.* reported a small bicarbonate desorption peak during temperature-programmed heating in CO ($25-620$ °C), however, no gas-phase CO_2 or IR bands of carbonates or bicarbonates were observed during CO exposure at 500 °C[45]. These observations suggest that formation of bicarbonates takes place below 500 °C, as expected based on the knowledge of bicarbonate species (for more information, see[28] and references therein).

5 Future perspectives

As both monoclinic zirconia and its interaction with CO have been investigated for more than 40 years, in some regions knowledge is still lacking. The surface configuration is one of the remaining questions, as the most stable surfaces according to density functional theory are different from those assumed based on HRTEM, yet the amount of independent experimental observations on clearly monoclinic samples remain few. The stability of the surface structure in the reaction conditions and during the reaction should be investigated carefully. Also the IR designation of terminal and multicoordinated hydroxyls (or any of the other interpretations) remains without irresputable evidence, even though the multi-oxide studies by Tsyganenko and Filimonov[3,71] were very thorough in providing comparable information of several oxides with presumably different OH groups due to their crystal structure. Especially in the light of theoretical calculations suggesting mostly terminal and bibridged hydroxyl species, further confirmation of the assignment would provide more clarity. The Zr cations (Zr^{3+}, Zr^{4+}) have also caused some confusion: the basis for the IR assignment is unclear, yet the trivalent species have

Catalysis Science & Technology Accepted Manuscript

This journal is © The Royal Society of Chemistry [year]

Table 7 Adsorbed or desorbed CO amounts reported in literature

Measurement	As reported	Scaled to μmol/m^2	T_{ads} °C	P_{CO}	t_{ads} min	Ref.
Adsorbed CO (MS)	0 μmol/g	0	25	5%	N/A	20
Adsorbed CO (MS)	10 μmol/g	0.050	150	5%	N/A	20
Adsorbed CO (MS)	26 μmol/g	0.13	250	5%	N/A	20
Adsorbed CO (MS)	37 μmol/g	0.19	350	5%	N/A	20
Desorbed CO_x (MS)	6.5 μmol/g	0.033	150	5%	N/A	20
Desorbed CO_x (MS)	23 μmol/g	0.12	250	5%	N/A	20
Desorbed CO_x (MS)	33.6 μmol/g	0.17	350	5%	N/A	20
Desorbed CO_x (MS)	0.09 μmol/m^2 (SA=19 m^2/g)	0.09	25	4%	20	30
Desorbed CO_x (MS)	0.17 μmol/m^2 (SA=19 m^2/g)	0.17	150	4%	20	30
Desorbed CO_x (MS)	0.22 μmol/m^2 (SA=19 m^2/g)	0.22	200	4%	20	30
Desorbed CO_x (MS)	0.35 μmol/m^2 (SA=19 m^2/g)	0.35	250	4%	20	30
Desorbed CO_x (MS)	0.51 μmol/m^2 (SA=110 m^2/g)	0.51	25	4%	20	30
Desorbed CO_x (MS)	0.46 μmol/m^2 (SA=110 m^2/g)	0.46	150	4%	20	30
Desorbed CO_x (MS)	0.59 μmol/m^2 (SA=110 m^2/g)	0.59	200	4%	20	30
Desorbed CO_x (MS)	1.34 μmol/m^2 (SA=110 m^2/g)	1.34	250	4%	20	30
Adsorbed CO (gravimetric)	$3-20\cdot10^{17}$ molec./m^2[a]	0.5 – 3.3[a]	500	1 atm	30	45
Net desorbed CO_x at 100 – 550 °C (MS)	240 – 530 μmol/g[b]	2.7 – 5.9[b]	100[b]	2%	90[a]	28

[a] Depending on sample preparation temperature (600 – 900 °C).
[b] Depending on pretreatment (hydration, reduction, reduction and hydration). CO contact first 90 min at 100 °C, then continuing during heating up to 550 °C.

been successfully probed with N_2O[6]. The EPR assignment of Zr^{3+} species has also been under discussion[8,46,47,51,57]. Further information on surface vacancies and also surface defects, *e.g.*, at the surface boundaries could give a more thorough look at the surface interaction with hydroxyl and CO species. Also tailoring the properties of monoclinic zirconia by using promoters and dopants without changing its crystalline phase could elucidate the interaction. Advanced methods similar to Raman in the case of ceria[93] might also provide surprisingly rich information.

With the adsorbed CO species the knowledge on especially the formate species deserves more investigation. The surface configuration of the species (monodentate, chelating or bridging bidentate) is unclear based on experimental observations, although bidentate species has been speculated and theoretical calculations suggest both chelating and bridging bidentate species. Also the enthalpy of formation for formate species has only been estimated theoretically, an experimental confirmation for it, *e.g.*, with microcalorimetry, would be welcome. Some clarity on the kinetics of formate formation on terminal and multicoordinated hydroxyls or even the extent of the reaction on both types of hydroxyls could provide new insights related to catalysis. Operando-style experiments with combined surface and gas-phase quantification would provide valuable input on all of the surface species with CO and hydroxyls. Observing the surface species in the same setup under vacuum might enlighten the mechanism of surface reduction *via* oxygen removal and why evacuation is a more efficient reduction method than hydrogen treatment[80].

To improve the modeling of carbon oxides, a better understanding of an active surface site is highly important to be able to set up more accurate computational surface models to better describe the complexity of the ZrO_2 support/catalyst. This would not only impact on calculation of adsorption energies but would also influence on calculated frequencies. As long as the nature of an active site is not known exactly, a systematic approach, where, *e.g.*, different surface models are investigated side by side, is a natural choice to obtain information of adsorption characteristics. To discover the active surface sites and to further improve the selectivity of catalysts, nanoshaped supports and catalysts with their surface regularity have proven an interesting alternative. The better the control over the surface sites, the better the catalyst selectivity. However, the control is only to be reached through monocrystalline nanoshapes as in polycrystalline shapes the surfaces are not controlled.

Growing monoclinic zirconia in the shape of nanofibres and nanorods has become gained some attention during the last 15 years, yet most of the shapes are polycrystalline. The preparation methods differ from traditional wet chemistry to prepare monoclinic zirconia powders. Nanorods have been prepared hydrothermally[16,17] in an autoclave, resulting in nanorods of various sizes, the diameter in general some tens of nanometers and the length a few hundred nanometers, and the length–

Catalysis Science & Technology Accepted Manuscript

diameter ratio ranging from *ca.* 5 up until 50 or even more.

Exposed faces of the nanoshapes should be characterized with advanced electron microscopy techniques (*e.g.* aberration-corrected TEM as in[94]) to determine the orientation of the exposed surfaces. Boucher *et al.*[95] have tested different shapes of metal oxides with gold catalysts for steam reforming of methanol and water-gas shift, and they conclude that the different shapes show somewhat different activities. Li and Shen[96] discuss widely the oxide shape effects in nanocatalysis, and they mention some of the unknown issues with metal deposition on oxide nanoshapes: whether the metal atoms are located on a single type of surface only. They also bring up that the nanoshapes might not be stable under the reaction conditions, this might also affect the metal–support interface, often considered to be the active site[96].

6 Conclusions

Monoclinic zirconia surface has three kinds of coordinatively unsaturated cationic sites, two types of Zr^{4+} and one type of Zr^{3+}, coordinatively unsaturated Zr^{4+}–O^{2-} pairs, oxygen vacancies, terminal hydroxyls, and two types of multicoordinated hydroxyl species. The ratios of these sites can be modified with pretreatments by removing or adding oxygen and hydrogen to the surface through applying heat, vacuum or reactive atmospheres. The cationic sites are responsible for the linearly adsorbed CO species while formates are suggested to form preferably on a site where an unshielded zirconium ion is paired with a terminal hydroxyl species, assuming a bidentate formate. This would provide an explanation for the submonolayer quantities of formate on zirconia. The concentrations of active sites for linear CO and formate formation are of similar magnitude, corresponding to *ca.* 5% of a monolayer or less, whereas the amount of hydroxyl species on the surface is roughly tenfold. The formates as well as hydroxyl species prefer the defect type of Zr^{4+} sites. The specific roles for Zr^{3+} and the terrace-type Zr^{4+} remain unclear. Other open questions include confirming the nature of the multicoordinated hydroxyls, the surface configuration of the formate species, and the energetics of formate formation. Nanoshapes might be a valuable tool in exploring the surface aspects related to formates and hydroxyls.

[a] *Department of Biotechnology and Chemical Technology, Aalto University School of Chemical Technology, P.O. Box 16100, 00076 Aalto, Finland. E-mail: sonja.kouva@aalto.fi*
[b] *Department of Chemistry, Nanoscience Center, University of Jyväskylä, P.O. Box 35, 40014 Jyväskylä, Finland*
[c] *Faculty of Science & Technology, University of Twente, P.O. Box 217, 7500 AE Enschede, The Netherlands.*

Acknowledgements

The authors acknowledge funding from Academy of Finland and Finland Distinguished Professor Programme (FiDiPro) funded by the Finnish Funding Agency for Technology and Innovation (TEKES).

References

1 K. Tanabe and T. Yamaguchi, *Catal. Today*, 1994, **20**, 185–198.
2 T. Yamaguchi, *Catal. Today*, 1994, **20**, 199–218.
3 A. A. Tsyganenko and V. N. Filimonov, *J. Mol. Struct.*, 1973, **19**, 579–589.
4 A. Christensen and E. Carter, *Phys. Rev. B*, 1998, **58**, 8050–8064.
5 D. V. Pozdnyakov and V. N. Filimonov, *Zh. Fiz. Khim.*, 1972, **46**, 1011–1012.
6 T. M. Miller and V. H. Grassian, *Catal. Lett.*, 1997, **46**, 213–221.
7 Z.-Y. Ma, C. Yang, W. Wei, W.-H. Li and Y.-H. Sun, *J. Mol. Catal. A: Chem.*, 2005, **227**, 119–124.
8 C. Morterra, E. Giamello, L. Orio and M. Volante, *J. Phys. Chem.*, 1990, **94**, 3111–3116.
9 A. Trunschke, D. L. Hoang and H. Lieske, *J. Chem. Soc., Faraday Trans.*, 1995, **91**, 4441–4444.
10 N. B. Jackson and J. G. Ekerdt, *J. Catal.*, 1986, **101**, 90–102.
11 J. Li, J. Chen, W. Song, J. Liu and W. Shen, *Appl. Catal., A*, 2008, **334**, 321–329.
12 C. A. Franchini, A. M. Duarte de Farias, E. M. Albuquerque, R. dos Santos and M. A. Fraga, *Appl. Catal., B*, 2012, **117-118**, 302–309.
13 G. Águila, S. Guerrero and P. Araya, *Catal. Comm.*, 2008, **9**, 2550–2554.
14 K. Takanabe, K. Aika, K. Inazu, T. Baba, K. Seshan and L. Lefferts, *J. Catal.*, 2006, **243**, 263–269.
15 M. Benito, R. Padilla, L. Rodríguez, J. Sanz and L. Daza, *J. Power Sources*, 2007, **169**, 167–176.
16 X.-L. Liu, I. Pappas, M. Fitzgerald, Y.-J. Zhu, M. Eibling and L. Pan, *Mater. Lett.*, 2010, **64**, 1591–1594.
17 R. Espinoza-González, D. Diaz-Droguett, J. Avila, C. Gonzalez-Fuentes and V. Fuenzalida, *Mater. Lett.*, 2011, **65**, 2121–2123.
18 C. Morterra, R. Aschieri and M. Volante, *Mater. Chem. Phys.*, 1988, **20**, 539–557.
19 M.-Y. He and J. G. Ekerdt, *J. Catal.*, 1984, **87**, 381–388.
20 D. Bianchi, T. Chafik, M. Khalfallah and S. J. Teichner, *Appl. Catal., A*, 1993, **105**, 223–249.
21 M.-Y. He and J. G. Ekerdt, *J. Catal.*, 1984, **87**, 238–254.
22 S. T. Korhonen, M. Calatayud and A. O. I. Krause, *J. Phys. Chem. C*, 2008, **112**, 16096–16102.
23 P. O. Graf, D. J. M. de Vlieger, B. L. Mojet and L. Lefferts, *J. Catal.*, 2009, **262**, 181–187.
24 W. Hertl, *Langmuir*, 1989, **5**, 96–100.
25 K. T. Jung and A. T. Bell, *J. Mol. Catal. A: Chem.*, 2000, **163**, 27–42.
26 F. Ouyang, A. Nakayama, K. Tabada and E. Suzuki, *J. Phys. Chem. B*, 2000, **104**, 2012–2018.
27 V. Bolis, C. Morterra, M. Volante, L. Orio and B. Fubini, *Langmuir*, 1990, **6**, 695–701.
28 S. Kouva, J. Andersin, K. Honkala, J. Lehtonen, L. Lefferts and J. Kanervo, *Phys. Chem. Chem. Phys.*, 2014, **16**, 20650–20664.
29 E. Guglielminotti, *Langmuir*, 1990, **6**, 1455–1460.
30 K. Pokrovski, K. T. Jung and A. T. Bell, *Langmuir*, 2001, **17**, 4297–4303.
31 A. V. Radha, O. Bomati-Miguel, S. V. Ushakov, A. Navrotsky and P. Tartaj, *J. Am. Ceram. Soc.*, 2009, **92**, 133–140.
32 S. V. Ushakov and A. Navrotsky, *Appl. Phys. Lett.*, 2005, **87**, 164103.

Catalysis Science & Technology Accepted Manuscript

This journal is © The Royal Society of Chemistry [year]

33 H. F. Holmes, E. L. Fuller Jr. and R. A. Beh, *J. Colloid Interf. Sci.*, 1974, **47**, 365–371.

34 J. Nawrocki, P. W. Carr, M. J. Annen and S. Froelicher, *Anal. Chim. Acta*, 1996, **327**, 261–266.

35 K. Dyrek, A. Adamski and Z. Sojka, Ceram. Interfaces 2, 2001, pp. 241–259.

36 K. Hadjiivanov, *Identification and Characterization of Surface Hydroxyl Groups by Infrared Spectroscopy*, Academic Press, 2014, vol. 57, pp. 99–318.

37 J. Nawrocki, M. P. Rigney, A. McCormick and P. W. Carr, *J. Chromatogr. A*, 1993, **657**, 229–282.

38 C. Morterra, L. Orio and C. Emanuel, *J. Chem. Soc., Faraday Trans.*, 1990, **86**, 3003–3013.

39 C. Morterra, L. Orio, V. Bolis and P. Ugliengo, *Mater. Chem. Phys.*, 1991, **29**, 457–466.

40 G. Cerrato, S. Bordiga, S. Barbera and C. Morterra, *Appl. Surf. Sci.*, 1997, **115**, 53–65.

41 K. T. Jung, Y. G. Shul and A. T. Bell, *Korean J. Chem. Eng.*, 2001, **18**, 992–999.

42 K.-D. Jung and A. T. Bell, *J. Catal.*, 2000, **193**, 207–223.

43 I. A. Fisher, H. C. Woo and A. T. Bell, *Catal. Lett.*, 1997, **44**, 11–17.

44 N. E. Tret'yakov, D. V. Pozdnyakov, O. M. Oranskaya and V. N. Filimonov, *Russ. J. Phys. Chem.*, 1970, **44**, 596–600.

45 R. G. Silver, C. J. Hou and J. G. Ekerdt, *J. Catal.*, 1989, **118**, 400–416.

46 M. J. Torralvo, M. A. Alario and J. Soria, *J. Catal.*, 1984, **86**, 473–476.

47 M. Anpo and S. C. Moon, *Res. Chem. Intermed.*, 1999, **25**, 1–12.

48 J. Kondo, H. Abe, Y. Sakata, K.-i. Maruya, K. Domen and T. Onishi, *J. Chem. Soc., Faraday Trans. 1*, 1988, **84**, 511–519.

49 J. Kondo, Y. Sakata, K. Domen, K.-i. Maruya and T. Onishi, *J. Chem. Soc., Faraday Trans.*, 1990, **86**, 397–401.

50 M. Bensitel, O. Saur, J. C. Lavalley and G. Mabilon, *Mater. Chem. Phys.*, 1987, **17**, 249–258.

51 E. Giamello, M. Volante, B. Fubini, F. Geobaldo and C. Morterra, *Mater. Chem. Phys.*, 1991, **29**, 379–386.

52 V. Bolis, G. Cerrato, G. Magnacca and C. Morterra, *Thermochim. Acta*, 1998, **312**, 63–77.

53 D. Bianchi, J.-L. Gass, M. Khalfallah and S. J. Teichner, *Appl. Catal., A*, 1993, **101**, 297–315.

54 X. Mugniery, T. Chafik, M. Primet and D. Bianchi, *Catal. Today*, 1999, **52**, 15–22.

55 O. Dulaurent and D. Bianchi, *Appl. Catal., A*, 2001, **207**, 211–219.

56 J. Erkelens, H. T. Rijnten and S. H. Eggink- Du Burck, *Recl. des Trav. Chim. des Pays-Bas*, 1972, **91**, 1426–1432.

57 M. G. Cattania, A. Gervasini, F. Morazzoni, R. Scotti and D. Strumolo, *J. Chem. Soc. Faraday Trans. 1*, 1989, **85**, 801–812.

58 K. Hadjiivanov and J.-C. Lavalley, *Catal. Comm.*, 2001, **2**, 129–133.

59 T. Yamaguchi, Y. Nakano and K. Tanabe, *Bull. Chem. Soc. Jpn.*, 1978, **51**, 2482–2487.

60 T. Yamaguchi, H. Sasaki and K. Tanabe, *Chem. Lett.*, 1973, **9**, 1017–1018.

61 P. A. Agron, E. L. Fuller Jr. and H. F. Holmes, *J. Colloid Interf. Sci.*, 1975, **52**, 553–561.

62 E.-M. Köck, M. Kogler, T. Bielz, B. Klötzer and S. Penner, *J. Phys. Chem. C*, 2013, **117**, 17666–17673.

63 T. Merle-Méjean, P. Barberis, S. B. Othmane, F. Nardou and P. E. Quintard, *J. Eur. Ceram. Soc.*, 1998, **18**, 1579–1586.

64 P. D. L. Mercera, J. van Ommen, E. B. M. Doesburg, A. J. Burggraaf and J. R. H. Ross, *Appl. Catal.*, 1991, **71**, 363–391.

65 K.-H. Jacob, E. Knözinger and S. Benfer, *J. Mater. Chem.*, 1993, **3**, 651–657.

66 D. Martin and D. Duprez, *J. Phys. Chem.*, 1996, **100**, 9429–9438.

67 S. T. Korhonen, M. Calatayud and A. O. I. Krause, *J. Phys. Chem. C*, 2008, **112**, 6469–6476.

68 G. Mogilevsky, C. J. Karwacki, G. W. Peterson and G. W. Wagner, *Chem. Phys. Lett.*, 2011, **511**, 384–388.

69 A. Ignatchenko, D. G. Nealon, R. Dushane and K. Humphries, *J. Mol. Catal. A: Chem.*, 2006, **256**, 57–74.

70 A. N. Kharlanov, E. V. Lunina and V. V. Lunin, *Russ. J. Phys. Chem.*, 1997, **71**, 1504–1509.

71 A. A. Tsyganenko and V. N. Filimonov, *Spectrosc. Lett.*, 1972, **5**, 477–487.

72 K. Yardley, *Mineral. Mag.*, 1926, **21**, 169–175.

73 D. K. Smith and W. Newkirk, *Acta Crystallogr.*, 1965, **18**, 983–991.

74 O. Syzgantseva, M. Calatayud and C. Minot, *J. Phys. Chem. C*, 2010, **114**, 11918–11923.

75 J. D. McCullough and K. N. Trueblood, *Acta Crystallogr.*, 1959, **12**, 507–511.

76 C. Warble, *Ultramicroscopy*, 1984, **15**, 301–309.

77 W. Piskorz, J. Gryboś, F. Zasada, S. Cristol, J.-F. Paul, A. Adamski and Z. Sojka, *J. Phys. Chem. C*, 2011, **115**, 24274–24286.

78 K. Momma and F. Izumi, *J. Appl. Crystallogr.*, 2011, **44**, 1272–1276.

79 M. C. Deibert and R. Kahraman, *Appl. Surf. Sci.*, 1989, **37**, 327–336.

80 K.-O. Axelsson, K.-E. Keck and B. Kasemo, *Appl. Surf. Sci.*, 1986, **25**, 217–230.

81 K.-H. Jacob, E. Knözinger and S. Benfer, *J. Chem. Soc., Faraday Trans.*, 1994, **90**, 2969–2975.

82 O. A. Syzgantseva, M. Calatayud and C. Minot, *J. Phys. Chem. C*, 2012, **116**, 6636–6644.

83 M. Van Thiel, E. D. Becker and G. C. Pimentel, *J. Chem. Phys.*, 1957, **27**, 486–490.

84 M. L. Cerón, B. Herrera, P. Araya, F. Gracia and A. Toro-Labbé, *J. Mol. Model.*, 2013, **19**, 2885–2891.

85 I. M. Iskandarova, A. A. Knizhnik, E. A. Rykova, A. A. Bagatur'yants, B. V. Potapkin and A. A. Korkin, *Microelectron. Eng.*, 2003, **69**, 587–593.

86 G. N. Vayssilov, M. Mihaylov, P. S. Petkov, K. I. Hadjiivanov and K. M. Neyman, *J. Phys. Chem. C*, 2011, **115**, 23435–23454.

87 F. Ouyang, J. N. Kondo, K.-c. Maruya and K. Domen, *J. Chem. Soc., Faraday Trans.*, 1996, **92**, 4491–4495.

88 G. Busca, J. Lamotte, J. C. Lavalley and V. Lorenzelli, *J. Am. Chem. Soc.*, 1987, **109**, 5197–5202.

89 G. Busca and V. Lorenzelli, *Mater. Chem.*, 1982, **7**, 89–126.

90 T. Shido and Y. Iwasawa, *J. Catal.*, 1992, **136**, 493–503.

91 T. Shido and Y. Iwasawa, *J. Catal.*, 1993, **141**, 71–81.

92 J. Zhu, J. van Ommen, H. Bouwmeester and L. Lefferts, *J. Catal.*, 2005, **233**, 434–441.

93 S. Agarwal, X. Zhu, E. J. M. Hensen, L. Lefferts and B. L. Mojet, *J. Phys. Chem. C*, 2014, **118**, 4131–4142.

94 S. Agarwal, L. Lefferts, B. L. Mojet, D. A. J. M. Ligthart, E. J. M. Hensen, D. R. G. Mitchell, W. J. Erasmus, B. G. Anderson, E. J. Olivier, J. H. Neethling and A. K. Datye, *ChemSusChem*, 2013, **6**, 1898–906.

95 M. B. Boucher, S. Goergen, N. Yi and M. Flytzani-Stephanopoulos, *Phys. Chem. Chem. Phys.*, 2011, **13**, 2517–27.

96 Y. Li and W. Shen, *Chem. Soc. Rev.*, 2014, **43**, 1543–74.

Catalysis Science & Technology Accepted Manuscript